

Water-binding strength as regulator of extracellular-matrix mechanics enables detection of swelling-associated biophysical alterations using MRI

Matthias R. Kollert

Berlin Institute of Health at Charité – Universitätsmedizin Berlin, Julius Wolff Institute & BIH Center for Regenerative Therapies, Berlin, Germany; Department of Health Sciences and Technology, ETH Zurich, Zurich, Switzerland

Martin Krämer

Institute of Diagnostic and Interventional Radiology, Jena University Hospital, Friedrich Schiller University Jena, Jena, Germany; Medical Physics Group, Institute of Diagnostic and Interventional Radiology, Jena University Hospital, Friedrich Schiller University Jena, Jena, Germany

Nicholas M. Brisson

Berlin Institute of Health at Charité – Universitätsmedizin Berlin, Julius Wolff Institute & BIH Center for Regenerative Therapies, Berlin, Germany

Victoria Schemenz

Department of Operative and Preventive and Pediatric Dentistry, Charité – Universitätsmedizin Berlin, Berlin, Germany

Serafeim Tsitsilonis

Berlin Institute of Health at Charité – Universitätsmedizin Berlin, Julius Wolff Institute & BIH Center for Regenerative Therapies, Berlin, Germany; Center for Musculoskeletal Surgery, Charité – Universitätsmedizin Berlin, Berlin, Germany

Taimoor H. Qazi

Department of Bioengineering, University of Pennsylvania, Philadelphia, PA, USA

Peter Fratzl

Department of Biomaterials, Max Planck Institute of Colloids and Interfaces, Potsdam, Germany

Viola Vogel

Department of Health Sciences and Technology, ETH Zurich, Zurich, Switzerland

Jürgen R. Reichenbach

Medical Physics Group, Institute of Diagnostic and Interventional Radiology, Jena University Hospital, Friedrich Schiller University Jena, Jena, Germany

Georg N. Duda (✉ georg.duda@charite.de)

Berlin Institute of Health at Charité – Universitätsmedizin Berlin, Julius Wolff Institute & BIH Center for Regenerative Therapies, Berlin, Germany; Center for Musculoskeletal Surgery, Charité – Universitätsmedizin Berlin, Berlin, Germany

Research Article

Keywords: ECM, viscoelasticity, osmolality, proteoglycans, swelling, water binding, hydration, MRI

Posted Date: July 19th, 2023

DOI: <https://doi.org/10.21203/rs.3.rs-3182367/v1>

License:  This work is licensed under a Creative Commons Attribution 4.0 International License.

[Read Full License](#)

Water-binding strength as regulator of extracellular-matrix mechanics enables detection of swelling-associated biophysical alterations using MRI

Matthias R. Kollert^{1,2}, Martin Krämer^{3,4}, Nicholas M. Brisson¹, Victoria Schemenz⁵, Serafeim Tsitsilonis^{1,6}, Taimoor H. Qazi⁷, Peter Fratzl⁸, Viola Vogel², Jürgen R. Reichenbach⁴, Georg N. Duda^{1,6}

1 Berlin Institute of Health at Charité – Universitätsmedizin Berlin, Julius Wolff Institute & BIH Center for Regenerative Therapies, Berlin, Germany

2 Department of Health Sciences and Technology, ETH Zurich, Zurich, Switzerland

3 Institute of Diagnostic and Interventional Radiology, Jena University Hospital, Friedrich Schiller University Jena, Jena, Germany

4 Medical Physics Group, Institute of Diagnostic and Interventional Radiology, Jena University Hospital, Friedrich Schiller University Jena, Jena, Germany

5 Department of Operative and Preventive and Pediatric Dentistry, Charité – Universitätsmedizin Berlin, Berlin, Germany

6 Center for Musculoskeletal Surgery, Charité – Universitätsmedizin Berlin, Berlin, Germany

7 Department of Bioengineering, University of Pennsylvania, Philadelphia, PA, USA

8 Department of Biomaterials, Max Planck Institute of Colloids and Interfaces, Potsdam, Germany

Abstract

Altered hygroscopic properties of the extracellular matrix (ECM), such as related to exudation, are characteristic for various pathologies including inflammation in injury, inherent swelling, or proteoglycan (PG) dysregulation. Mechanical properties of the ECM are key characteristics of various cell niches, capable of defining cell phenotype and fate, or of storing pathological information. Dehydration is known to alter ECM mechanics, but the role of the binding of water to the ECM remains unclear. Our data illustrate that the proportion of loosely to strongly bound water is a distinctive ECM property that regulates its mechanics and they suggest a crucial role of PGs for elastic and viscous characteristics. Osmolality and loosely bound water determine dynamic ECM properties. This understanding may pave the ground to diagnose related pathological tissue alterations non-invasively using combined MR T₁ and T₂^{*} mapping. Eventually, the strength of water binding may be utilized as controlled cell-niche property to guide cell behavior.

Keywords

ECM, viscoelasticity, osmolality, proteoglycans, swelling, water binding, hydration, MRI

Introduction

The extracellular matrix (ECM) of musculoskeletal tissues has crucial roles in physiology by providing stability to organs, scaffolding to cells, and enabling force transmission over long distances. Thereby, the ECM defines the physical cues acting on cells and guiding their behavior *in vivo*. Water is a main component of ECM and cells in living tissues (e.g., 62 wt% in tendon¹). It provides diffusivity, hydration and swelling pressure due to hygroscopic ECM properties². ECM hygroscopic properties are predominantly defined by proteoglycans (PGs), which play a key role in regulating tissue water content due to their high ion and water retaining capacity. They can generate osmotic pressures in the magnitude of 400 kPa, which is in the range of peak muscle stresses³⁻⁵. However, injury or diseases can disrupt these ECM properties and their function for cells. Various pathologies are characterized by osmotic dysbalances and related dysregulations, acute or chronic, of the involved ECM (e.g., deranged PG content or modified water binding), which are characteristic for inflammation⁶, swelling⁷, edema^{7,8}, some forms of cancer⁹⁻¹¹, and scarring^{12,13}. Within physiological limits, osmotic alterations regulate many essential processes in organs. For instance, osmotic pressure can strongly affect soft tissue tension and influence cell behavior¹⁴⁻¹⁷, or regulate swelling after injury or infection^{7,18}. So far, however, it remains unknown how osmotic dysregulation affects specifically the viscoelastic material properties of the ECM. Recently, viscoelastic properties of the ECM have been identified as being crucial for determining cell phenotype and fate and thereby guiding cell behavior (e.g., spreading, migration, differentiation¹⁹⁻²¹). Changes of these viscoelastic properties may indicate pathological tissue alterations (e.g., scarring, tumor progression^{11,21}).

But what defines these viscoelastic tissue properties? In the present study, we investigated if, and how, changes in the ion concentration of the local osmotic environment affect water binding in the ECM and through this, elastic and viscous characteristics of the ECM in a process distinct from the influence of ECM hydration. To this end, an *ex vivo* ECM model together with an experimental setup that allows to deliberately modulate the osmotic environment of a probe were developed and used to characterize the mechanical and structural properties of soft tissues, and to perform magnetic resonance imaging (MRI). The *ex vivo* ECM model is based on fresh, excised ovine Achilles tendon tissue, leveraging its organized structure to minimize potential confounding effects of diverse fiber directions on characterization measurements. Besides water, such tendon material mainly consists of collagen fibers and PGs, which are among the most abundant ECM proteins in physiology. Thus, characterization of tendon ECM as a model may lead to findings transferable to other tissue types²². To modulate swelling and water binding, thereby yielding distinct characteristics reflective of swelling-related pathologies, ECM samples were exposed to defined osmotic environments using ions or macromolecules as osmolytes. To detect changes in swelling and water binding non-invasively, we used quantitative MRI mapping to derive tissue relaxation parameters. These included T_1 and T_2^* , which can serve as biomarkers for tissue hydration²³⁻²⁵ and have previously been related to water binding in hydration layers around macromolecules in living tissues²⁶. We used T_2^* to detect alterations in the proportion of loosely to strongly bound water²⁷. To quantify viscoelasticity, we employed uniaxial compression²⁰. Multi-scale structural analysis was performed by histological staining, small-angle x-ray scattering (SAXS) and high-resolution MRI.

We hypothesized that the ion concentration of a local osmotic environment regulates ECM viscoelasticity by tuning water binding, and indeed we found this confirmed in mechanical, structural, and MRI characterization experiments. We aimed to reflect traits of swelling-related pathologies with the developed *ex vivo* ECM model and experimental setup, which we confirmed in a human case study with clinical *in vivo* MRI scans of a mechano-pathology (Achilles tendinopathy), thereby underscoring the clinical implications of our findings. The observed ECM alterations were distinct from effects of ECM dehydration, which we substantiated by using macromolecules as osmolytes and detailed structure analysis by SAXS.

MR relaxation parameters (T_1 and T_2^*) allowed to distinguish between distinct swelling-related ECM alterations and associated changes in biophysical properties (swelling, elastic modulus, and stress relaxation), as demonstrated by independent correlations, illustrating the potential of our results to eventually advance non-invasive diagnostics.

Results

In vivo scans of swelling-related pathological ECM alterations

To examine the potential of the employed ultra-short echo-time (UTE) MRI sequence for detecting swelling-related pathological ECM alterations, we mapped T_1 and T_2^* relaxation parameters within a clinical case study of *in vivo* MRI scans of one asymptomatic control subject (CTRL) and one patient diagnosed with mid-portion Achilles tendinopathy in their right foot (PATHO), a mechano-pathology caused by aberrant loading. For CTRL T_1 and T_2^* maps in the sagittal plane showed similar values for tendon mid-portions of left and right limb (Fig. 1a). In contrast, for PATHO, T_1 and T_2^* were increased in the sagittal plane in the tendinopathic right foot (warmer color, Fig. 1b). Subsequently, T_1 and T_2^* were quantified in tendon mid-portion volumes. T_1 was increased for PATHO (left: 959 ms, right: 1300 ms) in comparison to CTRL (left: 654 ms, right: 619 ms) (Fig. 1c, top). T_2^* was increased particularly in the patient's affected foot (left: 2.6 ms, right: 6.0 ms) in comparison to CTRL (left: 2.2 ms, right: 2.1 ms) (Fig. 1c, bottom). These values were in line with observations from parameter maps in the sagittal plane (Fig. 1b). Quantification of tendon mid-portion thickness showed increased values in the mid-portion in the patient's affected foot, suggesting tissue swelling (Supplementary Fig. 2). Notably, for the patient, T_1 values were also increased in the contralateral unaffected foot of the patient, likely due to compensatory gait leading to an onset of pathological ECM alterations.

Mid-portions of Achilles tendon as ex vivo ECM model and experimental setup

To enable controlled changes of ECM properties, fresh *ex vivo* mid-portions of Achilles tendons were analyzed next. We first compared MR relaxation parameters between whole tendon and dissected ECM samples. Fig. 2a shows fresh whole tendon (left) and the associated T_1 (middle) and T_2^* (right) maps of a representative tendon cross-section. T_1 and T_2^* increased from the enthesis to the calcaneus (bottom). In the mid-portion of the tendon, T_1 and T_2^* remained constant. Subsequently, ECM samples were dissected from tendon mid-portions and imaged anew in freshly dissected condition (FRESH) in our 3D printed mounting device (Fig. 2b, left). The observed T_1 and T_2^* (purple, blue) in parameter maps (Fig. 2b, middle and right) were similar to those observed for whole tendon mid-portions (Fig. 2a). Quantification of these values in whole tendon mid-portion and ECM sample volumes confirmed no significant difference with T_1 of 329 ms versus 314 ms (Fig. 2c) and T_2^* of 0.208 ms versus 0.212 ms (Fig. 2d). The developed experimental setup enables consistent ECM-model properties, modulation of the osmotic environment, and alignment of ECM fiber orientation (Fig. 2e). The latter was required especially for reproducible MRI characterization. The setup allows to combine ECM characterization for structure, mechanics, osmotic environments and MR relaxation parameters to investigate the interplay between osmolality, swelling and water binding, and their effects on viscoelasticity.

T_1 and T_2^ mapping of freshly dissected tissue samples reveals osmolality-tuned ECM water binding*

To investigate how osmotic environments affected ECM hydration and water binding, T_1 and T_2^* mapping was performed *in vitro*. Using the described experimental setup, we tested the incubation time required to reach swelling equilibrium for freshly dissected ECM samples exposed to hypo-osmolar (HYPO) or iso-osmolar (ISO) solutions, showing equilibrium was reached after 6 h (Fig. 2f). To ensure equilibrium swelling and feasibility of measurement logistics, incubation time was set to 24 h for all subsequent

experiments. ECM samples swelled in both HYPO and ISO after 24 h (Supplementary Fig. 5). T_1 increased for HYPO (410 ms) and ISO (491 ms) compared to FRESH (314 ms) (Fig. 2g). T_2^* remained unchanged in HYPO (0.197 ms), whereas it increased in ISO (0.349 ms), compared to FRESH (0.212 ms) (Fig. 2h), showing characteristics different to T_1 . However, results for T_1 and T_2^* suggest that water uptake in HYPO was strongly bound within the ECM, presumably by PGs, whereas in ISO an increased proportion of loosely bound water was present. In contrast, increasing environmental ion concentration from ISO by 26% and 100% did not change T_1 , T_2^* or swelling compared to ISO (Supplementary Fig. 6a–c). This suggests that in ISO strongly bound water was already at a low level and that the decreasing effect on water-binding strength by higher environmental ion concentrations had saturated. This observation supported the experimental design focusing on the comparison between HYPO and ISO conditions to yield low or high proportions of loosely to strongly bound water, respectively. The pronounced difference in water binding between the conditions facilitated investigating their effects on ECM structural and mechanical properties. The increases of T_1 , T_2^* and swelling from FRESH to ISO showed similar characteristics to those observed in the in vivo scans of CTRL versus PATHO (Fig. 1a–c, Supplementary Fig. 2), suggesting that our ex vivo ECM model with osmotic environment modulation has the potential to reflect traits of pathological ECM alterations.

ECM structure is altered by osmotic modulation

To better understand causes of observed changes in MR relaxation parameters that indicated increased proportions of strongly bound water in HYPO condition, we analyzed the microscopic structure in representative ECM cross sections using H&E and AB histological stainings. H&E images showed light lines at tendon fascicle edges²⁸ and were clearly expanded in HYPO, with parts of the delicate interfascicular (IF) matrix having been flushed away during the staining process, leaving unstained spaces (Fig. 3, top). AB images showed increased PG density in and around the IF connective tissue, as expected, compared to the collagen-rich fascicles (Fig. 3, middle). The expanded PG-rich IF regions in HYPO, visible in H&E and AB, suggested that PGs bound more water compared to FRESH and ISO conditions.

To verify this histological finding, we used MRI high resolution imaging with a 9.4 T scanner to obtain non-invasive insight into the tissue structure (Fig. 3, bottom). Light voxels depicted high signal intensities associated with increased amounts of water. MRI scans showed white lines with high signal intensity for tissue in HYPO, contrasting FRESH and ISO, which corresponded to a width of 70–140 μm and thus were of similar magnitude as the approximately 100 μm wide expanded IF regions in H&E and AB stainings. Taken together, the histological stainings and high resolution MR images indicate that ECM alterations in HYPO condition are due to increased water binding by PGs.

ECM mechanics are regulated by osmolality-tuned water binding

To understand the effects of the osmolality-tuned water binding and swelling on viscoelasticity of dissected Achilles tendon, bulk mechanical properties of ECM samples were quantified. The elastic modulus E of ECM samples increased from FRESH (136 kPa) to HYPO (198 kPa) and decreased in ISO (57 kPa) condition (Fig. 4a). These changes suggested that increased amounts of strongly bound water in HYPO led to higher compressive resistance of ECM samples. In contrast, increased amounts of loosely bound water in ISO (Fig. 2d and f), showed decreased E . Such decrease in E for iso-osmolar swelling is in line with recent findings for spine-disk samples²⁹.

To further analyze the ECM stress-relaxation behavior, the dissipation of applied stress over time was recorded. Representative stress relaxation curves of HYPO and ISO conditions in comparison to FRESH condition (resembling physiological tissue more closely), showed faster and slower decays, respectively, reflecting the influence of the different osmotic environments (Fig. 4b). Subsequently, stress relaxation

properties were quantified using stress relaxation half time $\tau_{0.50}$, a widely applied parameter in biomaterial and tissue engineering²⁰. We found a strong decline from FRESH (483 s) to HYPO (245 s), while values remained at similar levels in ISO (483 s) condition (Fig. 4c). Further insight into ECM stress-relaxation behavior was achieved by using $\tau_{0.65}$, reflecting the early dissipation of applied stress. $\tau_{0.65}$ decreased from FRESH (76 s) to HYPO (15 s) and, in contrast, increased in ISO (156 s) condition (Fig. 4d). In contrast, when the environmental ion concentration was increased by 26% and 100% relative to ISO condition, ECM mechanics did not change compared to ISO condition (Supplementary Fig. 6d–f). In these two conditions of increased ion concentrations, swelling and water-binding strength were at levels comparable to ISO (Supplementary Fig. 6a–c). Together with the absence of clear changes in ECM mechanics, these observations support the notion that changes in water binding caused the significant differences in ECM mechanics between HYPO and ISO conditions. These results demonstrate that environmental ion concentrations tuned ECM mechanics by altering the proportion of loosely to strongly bound water, with HYPO leading to higher elastic moduli and faster stress relaxation compared to ISO.

To verify that observed changes in mechanics were due to ECM components (e.g., PGs) and not potential influences of cells in the tissue (e.g., contractile forces), two additional experiments were performed. Alternating exposure of ECM samples to HYPO and ISO solutions showed the reversibility of viscoelasticity changes (Supplementary Fig. 7). Further, ECM samples used initially for MRI characterization (Fig. 2) were then also characterized mechanically, five days after excision, with storage and incubation between measurements at 4 °C. Mechanical characterization showed viscoelastic properties in HYPO and ISO conditions similar to those in ECM samples already analyzed two days after excision (Supplementary Fig. 8). Both experiments suggest that ECM components caused the observed changes in viscoelasticity.

Alterations in ECM swelling and viscoelasticity can be distinguished by combined T_1 and T_2^ mapping*

Next, the aforementioned measurement datasets were analyzed for independent correlations to elucidate the potential to non-invasively detect alterations in ECM swelling and viscoelasticity based on changes in MRI T_1 and T_2^* . Correlations were based on observed changes of each parameter between FRESH, HYPO and ISO conditions, denoted by Δ . For ΔT_1 , a positive correlation was found with Δ swelling ($r=0.84$), but not with viscoelastic parameters ΔE ($r=-0.05$) or $\Delta\tau_{0.65}$ ($r=-0.06$) (Fig. 5a–c). In contrast, ΔT_2^* did not correlate with Δ swelling ($r=0.30$), but instead negatively correlated with ΔE ($r=-0.74$) and positively correlated with $\Delta\tau_{0.65}$ ($r=0.76$) (Fig. 5d–f). The used MR relaxation parameters have been used previously as markers for disease and regeneration. These independent correlations demonstrate the potential of combining T_1 and T_2^* to distinguish between alterations in ECM swelling and water binding (e.g. in pathological ECM alterations) and related changes of ECM viscoelasticity (e.g., E , $\tau_{0.65}$), as schematically shown in Fig. 5g. As another, potentially more user-friendly, way to gain information about the characteristics of ECM alterations from T_1 and T_2^* measurements, we defined the parameter *SwellChar* to integrate the relationship of the MR-parameter changes: $SwellChar = \Delta T_1 \wedge (\Delta T_2^*)$. The application of *SwellChar* to the present data set yielded two Q_1 – Q_3 value ranges: [0.77–1.3] and [1.6–2.5]. Q_1 and Q_3 related to distinct swelling characteristics of high and low proportions of strongly bound water, respectively, with correspondingly increased or decreased viscoelasticity (Fig. 5h). Thus, *SwellChar* enabled the interpretation of combined T_1 and T_2^* measurements regarding their meaning for ECM biophysical properties using only one read-out.

Tissue dehydration leads to different ECM mechanics and different T_2^ signal*

Hyper-osmolar conditions can occur in physiology and pathology, with one scenario being increased osmotic pressure with effects similar to tissue dehydration (e.g. solid-tumor environments^{11,30}). To better understand how altered molecular crowding affects ECM properties in comparison to altered water-binding

strength, as shown above, ECM samples were subjected to different concentrations of macromolecules (PEG). These uncharged macromolecules exert osmotic pressure on ECM samples as they are unable to diffuse into ECM samples, in contrast to ions in the solution (Fig. 6a). PEG was added to HYPO and ISO solutions in concentrations to yield osmotic pressures of 100 and 200 kPa, magnitudes shown previously to be physiologically relevant (e.g., regulating stem cell fate^{16,17}). It should be noted that the ion concentration of ISO solution had an equivalent osmotic pressure of 744 kPa. With PEG-induced osmotic pressures, samples showed effects of dehydration with swelling decreased for 100 and 200 kPa in HYPO (17%, 27%) and for 200 kPa in ISO (34%) (Fig. 6b). Osmotic pressures of 200 kPa increased E in ISO (160%) (Fig. 6c), with the change of E in ISO in line with previous studies on tissue dehydration^{14,29}. $\tau_{0.65}$ decreased for 200 kPa in HYPO (45%) and for 100 and 200 kPa in ISO (85%, 92%) (Fig. 6d). T_1 decreased for osmotic pressure of 100 kPa in HYPO (13%), and for both pressures in ISO (19%, 25%) (Fig. 6e), which was in line with its aforementioned correlation with swelling (Fig. 5a). T_2^* increased substantially with applied osmotic pressure in both HYPO (252%, 266%) and ISO (252%, 216%) (Fig. 6f). These increases in T_2^* clearly exceeded the 65% increase observed when comparing FRESH to ISO (Fig. 2f) that resulted in clearly decreased viscoelasticity (Fig. 4). In HYPO, swelling and T_1 appeared to decrease less at 200 kPa osmotic pressure than in ISO. This was in line with increased amounts of strongly bound water in HYPO leading to higher swelling pressure within the ECM, and thus to enhanced resistance to the applied mechanical (as seen with E) or osmotic (as seen with swelling) compression. The observations that osmotic pressure increased viscoelasticity in HYPO and ISO suggests that water binding regulates viscoelasticity independently from (de)hydration, thus involving a different mode of osmolality-ECM interaction. The particularly large increase in T_2^* in PEG conditions suggests that combined T_1 and T_2^* mapping could have the potential to distinguish ECM alterations caused by applied osmotic pressure from alterations related to swelling and altered water binding. The greater change in T_2^* could be caused by effects of dehydration, previously shown capable of causing collagen-fiber contraction and, thus, tissue contraction¹⁴. These findings are significant, as understanding the differential effects of osmotic pressure (or mechanical loading)-induced tissue contraction, altered water-binding strength, and swelling could potentially be useful for distinguishing different tendon pathologies.

Diffusion of monovalent ions regulates ECM viscoelasticity through proteoglycans (PGs)

To elucidate how environmental ion concentrations regulate water binding and, consequently, viscoelasticity, we first used a stepwise osmotic gradient between HYPO and ISO conditions. Measurements revealed an increasing normalized ion efflux from ECM samples with decreasing baseline osmolality (Fig. 7a), reflected by their negative correlation ($r=-0.90$). To verify that the ion effluxes were related to viscoelasticity changes, ECM mechanics were characterized after incubation. Viscoelasticity was found to increase with decreasing baseline osmolality (Fig. 7b–c), reflected by a negative correlation for E ($r=-0.94$) and a positive correlation for $\tau_{0.65}$ ($r=0.89$).

To distinguish between potential effects of collagen fiber contraction due to osmotically induced structural alterations in ECM viscoelasticity in HYPO versus ISO conditions, SAXS was used. The axial staggering of tropomolecules in collagen fibrils results in a periodic pattern of stripes with higher (overlap) and lower (gap) molecule density that can be imaged by transmission electron microscopy (TEM) or SAXS^{31,32}. The collagen axial staggering was evaluated by analyzing the two-dimensional (2D) SAXS patterns which showed several orders of Bragg peaks (Fig. 7d). The n -th q positions ($n = 1, 3, 5, \dots$) can be converted to $D = 2\pi n/q_n$, where D is the intermittent distance (~ 67 nm) inside the collagen fibrils as indicated by gap and overlap zones. Analysis of the peak positions of signal intensities in the q space showed no relevant shift of peak positions between the two conditions (Fig. 7e). The absence of a relevant shift between the peaks shows that collagen fibers did not contract, suggesting no induced tensile stresses by axially contracting

collagen fibers that may have affected ECM mechanics¹⁴. Further, the lateral packing of collagen molecules was analyzed from 2D SAXS patterns (Fig. 7f) and revealed a slightly increased spacing in HYPO compared to ISO (Fig. 7g). This indicates a somewhat higher water content in fibrils subjected to HYPO condition.

To understand the role of PGs, that reside in the perifibrillar matrix around collagen, in regulating the observed changes of ECM viscoelasticity, the diffusion of ions out of ECM samples was investigated next. Comparing HYPO versus ISO, first the ion efflux was measured in terms of osmolality change after incubation (24h) and with respect to baseline (base) solutions. Osmolality increased only in HYPO, suggesting ion efflux from ECM samples (Fig. 7h). In contrast, there was no change in after incubation in ISO. Monovalent and divalent cations can bind to negatively charged PGs and affect their function and charge density³³. For example, Na^{1+} can neutralize PG negative charge and Ca^{2+} can form inter-chain cross-links between PGs. Subsequently, we measured concentrations of selected ions, Na^{1+} , Cl^{1-} , K^{1+} , Ca^{2+} and Mg^{2+} , in HYPO and ISO solutions after 24 h of ECM sample incubation (HYPO_{24h}, ISO_{24h}). From solution ion concentrations, we aimed to detect potential ion efflux and thus, alterations inside ECM samples. Notably, base solutions were deionized water (HYPO) and physiological saline solution without Ca^{2+} and Mg^{2+} (ISO). In HYPO_{24h}, concentrations of monovalent ions Na^{1+} , Cl^{1-} and K^{1+} were increased, while divalent ions Ca^{2+} and Mg^{2+} were at very low concentrations (Fig. 7i). This suggests that divalent cations mostly remained inside the ECM due to the higher strength of divalent ion bonds, in contrast to monovalent cations diffusing out. In ISO_{24h}, Na^{1+} , Cl^{1-} and K^{1+} were overall at comparably high concentrations (Fig. 7j), which was expected as the baseline solution, ISO, contained these ions. Interestingly, also in ISO divalent ions Ca^{2+} and Mg^{2+} remained at very low levels. The low concentrations of Ca^{2+} and Mg^{2+} in both HYPO_{24h} and ISO_{24h} solutions suggest that their tighter divalent bonds inside the ECM prevented their efflux. This is despite the abundantly available monovalent cations, such as Na^{1+} , that could have replaced bonds of divalent ions, such Ca^{2+} .

Discussion

Inflammation or injury of the ECM causes swelling and associated alterations of tissue properties. In this work, pathological alterations of Achilles tendon were selected as a model to investigate related changes in ECM biophysical properties and methods to detect such changes non-invasively. While clear differences between healthy and inflamed tendon can be captured with MRI (Fig. 1), little is known about the physical causes that result in the significant differential alterations of T_1 and T_2^* . Our systematic study of dissected tissues exposed to defined osmotic environments provides highly valuable insights by improving the understanding of fundamental ECM properties, thereby enabling a more advanced interpretation of MRI scans. Our data show how osmotic environments differentially regulate ECM swelling, water binding (Fig. 2) and viscoelasticity (Fig. 4), and unravels the role of the perifibrillar matrix, namely PGs (Fig. 7), for regulating water binding and ECM mechanics. We have shown that the environmental ion concentration regulates water binding, and that the state of this water binding plays a crucial role in ECM elasticity and stress relaxation (Fig. 4). Our ex vivo ECM model and experimental setup with osmotic environment modulation enabled parallel characterization of mechanical properties and MR relaxation parameters (Fig. 2). Therein, we used a well-controlled ECM model based on fresh biological tissue instead of artificial material to mimic an in vivo setting more accurately, which was supported by an in vivo case study comparing a healthy control subject to a patient. We presented a novel approach for non-invasive detection of observed ECM alterations using combined T_1 and T_2^* mapping, and identified their independent correlations with ECM biophysical properties, including swelling, elasticity, and stress relaxation. Further, we demonstrated the collagen-independent role of PGs in ECM viscoelastic properties (Fig. 7), and that environment ion concentration and osmotic pressure regulate ECM viscoelasticity differently (Fig. 6). We believe our findings may help to advance methods for non-invasive detection of local ECM alterations in

pathologies involving dysregulations of osmotic environments, PGs in the periferibrillar matrix, swelling and water binding, as well as synthetic biomaterial-based therapeutic approaches.

The observed increased viscoelasticity of ECM samples in conditions with increased proportions of strongly bound water is a particularly important finding as stress-relaxation properties of physiological, viscoelastic ECM were previously identified as a crucial driver for cell-matrix interactions (e.g., stem cell fate decision in regeneration)^{20,21}. On the contrary, decreased stress relaxation, observed in conditions with decreased water binding, was previously related to pathological ECM degeneration³⁴⁻³⁶, and may also be related to dysregulated water binding. The elastic modulus was already found to regulate the abovementioned governing cell functions³⁷, and its various roles in physiology continue to be investigated. In the context of hypo-osmolar environments, a recent study by Lee et al. reported that these environments regulate cell-fate decision in regeneration using viscoelastic ECM-mimicking hydrogels¹⁷. However, they did not consider potential effects of decreased environmental ion concentration on ECM viscoelasticity, although faster relaxation could have stimulated cells similarly¹⁷.

To understand the causes of the presented strong alterations in ECM mechanics observed for altered environmental ion concentration (i.e., HYPO versus ISO), common paradigms might have considered influences of load-bearing collagen fibers (i.e., osmotic-pressure induced tensile stress¹⁴) or cells, either actively (e.g., contractile forces³⁸) or passively (e.g., protein-phosphorylating cytosolic enzymes³⁹). However, SAXS analyses of collagen molecule axial staggering and lateral packing revealed that collagen likely did not contribute to the observed alterations in ECM mechanics. This finding was in line with a previous study showing that collagen fibers in aqueous solutions relax to maximum length at zero and low ion concentrations⁴⁰. Cellular influences were considered negligible as storage and incubation conditions (i.e., low temperatures, without nutrients) likely rendered cells apoptotic or inactive and impaired efficient enzyme function. Moreover, differences in ECM mechanics were maintained after alternating exposure to HYPO (dH₂O) and ISO solutions, likely leaving cells apoptotic. Further, cells would not be able to cause the observed strong changes in ECM mechanics even in ideal culture conditions³⁸.

By investigating the diffusion of selected ions that can affect PG function, the role of PGs in ECM viscoelasticity was shown (Fig. 7). Ion efflux from ECM samples correlated with viscoelasticity alterations. A significant efflux of monovalent cations, such as Na¹⁺, in low osmolality (i.e., HYPO) condition suggested more negatively charged PGs, leading to an increased proportion of strongly bound water in the periferibrillar PG-matrix³³. The negative charge of PGs is generated predominantly by their numerous subunits, chondroitin-sulfate (CS) chains, and an increased negative charge was previously found to result in stacking of CS chains due to electrostatic repelling effects³³. In contrast, measurements of divalent cations suggested that Ca²⁺ ions, for example, stayed bound inside ECM samples where these can form dynamic inter-chain cross links between PGs³³, which can affect ECM viscoelasticity²⁰. Our data suggest that in conditions of increased PG negative charge (e.g., HYPO), electrostatic repelling effects between PGs act as steric hindrance and increase the flexibility of dynamic Ca²⁺ inter-chain crosslinks, which consequently increases ECM stress relaxation under mechanical load²⁰ (Fig. 8). Further, the data suggest that increased proportions of strongly bound water results in increased swelling pressure² and, consequently, increased compressive resistance of the ECM.

Dynamic microscopic ECM properties, particularly viscoelasticity, have gained considerable attention recently in tissue engineering for enabling cells to actively remodel their surroundings and expand the range of more established macroscopic ECM properties, such as load-bearing fiber structures that provide stability and scaffolding functions^{21,41}. In this context, viscoelasticity is often considered to be regulated by the extent of covalent crosslinking in the matrix. Hygroscopic properties have been considered mainly as a prerequisite to yield a hydrated fiber network for mimicking natural ECM (e.g., with hydrogels)⁴¹.

However, the presented results highlight the role of the perifibrillar (PG-rich) matrix to regulate ECM viscoelasticity. In this context, we propose that the PGs' function as key regulator of ECM water binding may expand the list of mechanobiological cues for cell-matrix interactions (e.g., mechanics, fiber structure, porosity, topography). Disease modeling of pathologies involving dysregulations of PG function, osmotic environments or swelling can be potentially improved using ECM-mimicking materials that allow to modulate water-binding strength. Such an approach may enable to investigate its potential role in misguiding cell behavior in pathology and identify novel therapeutic targets.

While MRI allows to distinguish inflamed ECM (e.g., tendinopathy) from healthy ECM, it is difficult to non-invasively detect associated mechanical changes. Understanding the local mechanical competence of the tissue could help to unravel the causes for poor tendon healing outcomes that many patients experience. Our findings allow an improved interpretation of MRI data, leveraging a link between PG water binding and viscoelasticity and independent correlations of T_1 and T_2^* with swelling and viscoelasticity, respectively. For example, in our *in vivo* case study (Fig. 1), MRI of the patient's pathological Achilles tendon could be interpreted as severe swelling with decreased viscoelastic properties, indicating altered tissue composition and impaired functionality. The patient's contralateral and presumably healthy Achilles tendon showed an increase in T_1 only, suggesting an onset of pathological alteration characterized by first inflammatory swelling, caused by cytokine-mediated exudation. Viscoelasticity, and thus functionality and tissue composition, appears maintained. Such insight could support orthopedic surgeons in prescribing a suitable therapeutic approach for the patient, for instance, personalized physiotherapy addressing compensatory gait mechanics that may have led to the pathological tissue alterations in the unaffected contralateral foot due to aberrant loading patterns. Another example is the improvement of surgical interventions for degenerated or ruptured Achilles tendon. To date, it is not well understood why for some patients healing of sutured ends of a tendon leads to scarring or non-union, accompanied by diminished mechanics and functionality. Our data could facilitate better monitoring of healing progress after surgery and help recognize and categorize impaired tissue regeneration earlier. This could allow for improved clinical decision making, before significant tissue degeneration adapting physiotherapy protocols, or deciding for corrective surgery, before significant tissue degeneration when intervention success rates may be greater. Furthermore, we showed clearly distinguishable characteristics in MRI for osmotic pressure (PEG) induced ECM dehydration compared to altered water binding (i.e., HYPO versus ISO). This may support the use combined T_1 and T_2^* mapping for identifying disease-specific tissue degeneration. For instance, previous studies have shown that expanding solid tumors compress and dehydrate surrounding soft tissue^{11,30}. ECM water binding and other biophysical properties (e.g., swelling, mechanics) are important markers in various pathologies (e.g., viscoelasticity in glioblastoma³⁵, hypertension³⁶, intervertebral disc³⁴; fluid accumulation in lung inflammation⁶, swelling⁷, edema^{7,8}) and in regeneration (e.g., return to sport after surgery, personalized therapy, judging therapy impact).

This work demonstrates the crucial role of water binding for elastic and viscous characteristics of the extracellular matrix. Osmotic environments were shown to modulate the ECM water-binding properties and suggest an important role of proteoglycans to regulate proportions of loosely to strongly bound water in tendon tissue. Our investigations revealed independent correlations of MRI T_1 and T_2^* with ECM swelling and viscoelasticity, respectively, showing the potential of their combined application to discriminate pathological tissue alterations related to dysregulated swelling, water binding or osmotic environments. Future work should investigate this potential with *ex vivo* tissue probes of pathologically degenerated tissue and *in vivo* scans from a larger cohort of patients. Shedding light on the interplay between water binding and mechanics may lead to novel tissue engineering strategies involving biomaterials that enable controlling their hygroscopic properties as one dynamic microscopic design parameter.

Materials and methods

The part of this work involving human participants was approved by the Ethics Board of the Charité – Universitätsmedizin Berlin (EA2/088/16). All subjects provided written informed consent. For the ex vivo analyses, tissue samples were harvested from animals after euthanasia in compliance with the ethical guidelines of legal, local animal rights protection authorities (Landesamt für Gesundheit und Soziales Berlin). To keep the number of animals to a minimum, the samples were taken from other research projects but with no relationship that would affect tissue properties of the samples (G0424/17, G0210/18).

In vivo scans

In vivo imaging was performed with a clinical 3 T whole-body MRI scanner (MAGNETOM Vida, Siemens Healthineers) using a 16-channel measurement coil for foot and ankle scans as commonly used in clinical application (Foot/Ankle 16, Siemens Healthineers). Imaging was performed separately for each foot in two individuals: one healthy asymptomatic control subject (male, 34 y) without known pathologies (CTRL) and one patient (female, 53 y) with mid-portion Achilles tendinopathy (PATHO) diagnosed by a Senior Consultant (S.T.) for surgery (Supplementary Fig. 1a). The same UTE imaging sequence, described in more detail below, was used for the in vivo and ex vivo measurements, with five flip angles ranging from 5° to 24° for VFA based T₁ mapping and three echoes from 0.1 to 4.8 ms TE for T₂^{*} mapping. The UTE sequence was optimized for image acquisition of tendon tissue, potentially resulting in erroneous T₂^{*} values for non-tendon tissues with transverse relaxation times clearly longer than 5 ms. Fewer echoes were selected compared to the ex vivo acquisition to reduce acquisition time and patient discomfort. Both acquisitions used spatial resolution of 1.2 x 1.2 x 3.5 mm³ and acquisition bandwidth of 1076 Hz/pixel, with a TR of 12 ms for T₁-related and 8 ms for T₂^{*}-related data acquisition. Analysis was performed as for the ex vivo study.

Ex vivo ECM model

Fresh Achilles tendons were excised from 16 healthy sheep (Merino, female, 4+ y). The tissue samples were subdivided into different experiments, as displayed in Supplementary Fig. 1b. To avoid dehydration, tendons were enveloped in plastic wrap, placed in a moist environment immediately after excision, and stored at 4 °C until dissection and testing. A moist environment was established by placing each tendon in a sealed 50 ml polypropylene centrifuge tube with water-moistened cotton gauze at the conical tip of the tubes. Achilles tendon consists of two distinct bands of fibrous tissue connecting each of the gastrocnemius and soleus muscles via the enthesis to the bone. The gastrocnemius band was used due to its mostly elongated cylindrical shape, allowing for similar ECM sample sizes and better tissue handling during characterization (e.g., fiber direction for MRI, and parallel planes for mechanical characterization). Tendon samples from the contralateral limbs were assumed to have comparable tissue properties to the ipsilateral limbs. To avoid cartilaginous or calcified structures near the enthesis, diverse fiber directions in the transition from mid-tendon to enthesis, or myofibrous structures near the muscle, only the mid-portion of a tendon was used. The tendon mid-portion was defined between ~2.5 cm to ~5 cm distal to the enthesis. Each tendon mid-portion was then dissected cross-sectionally into six to eight cylindrical ECM samples of ~3 mm thickness. The tendon mid-portion's elongated shape, ordered structure, and consistent tissue properties allowed the variability of ECM structure and components to be minimized. ECM samples were characterized at room temperature and in fresh condition as MR relaxation parameters can be affected by freeze-thawing⁴² or fixation⁴³.

Osmotic environment modulation

Mechanical and MRI characterizations were performed directly after dissection (i.e., FRESH condition) and again after swelling in different osmotic environments for 24 h, as depicted in Supplementary Fig. 3.

For exposure to different osmotic environments, a 15 ml tube containing 8 ECM samples carried by 3D printed poly(chitosan-g-lactic acid) (PCLA) inlays that allowed contactless sample positioning and unconfined swelling (Fig. 2b) was filled with 13 ml of the respective solution. To tune ECM properties through the osmotic environment of a sample (i.e., the ion concentration of the bath solution), the hypo-osmolar environment was established with deionized water (HYPO) and the iso-osmolar environment with physiological saline solution without Ca^{2+} and Mg^{2+} (ISO) (D8537, Sigma-Aldrich) with a pH value ~ 7 . For hyper-osmolar environments, osmolality was either increased by saline concentration for higher ion concentration, or by adding macromolecules for dehydration of ECM samples by osmotic pressure. For higher ion concentration, saline concentrations were increased by 26% and 100% (double ISO osmolality). Van't Hoff's equation was used to determine the osmotic pressure in pascals $\pi = cRT$, with c , R and T representing the osmolar concentration of the solute, the gas constant, and the absolute temperature, respectively. Accordingly, ion concentration increases by 26% and 100% corresponded to osmotic pressure increases of ~ 200 kPa and ~ 744 kPa, respectively. For dehydration, we added 5 kDa polyethylene glycol (PEG) molecules (06679; Sigma-Aldrich Inc.), which cannot diffuse into the samples, to the swelling solutions, and thus apply osmotic pressure¹⁴. For PEG in aqueous solutions, osmotic pressure was calculated as previously described⁴⁴: PEG concentrations of 91 g/L and 125 g/L yielded osmotic pressures of ~ 100 kPa and ~ 200 kPa, respectively.

MRI UTE imaging for T_1 and T_2^ mapping*

MRI scans to characterize ECM samples in FRESH condition were performed after 3 days of storage, and subsequently, after 24 h exposure to different osmotic environments. To avoid dehydration of ECM samples in FRESH condition during the MRI scans taking 1 to 3 hours, water-moistened gauze was placed in the bottom of a sealed 15 ml tube carrying a PCLA inlay without contact to ECM samples (Supplementary Fig. 4). The 3D printed PCLA inlays served as a mounting device to hold ECM samples in parallel contactless positions (Fig. 2b)⁴⁵. For MR data acquisition, multiple tubes containing all ECM samples at a given time point were measured simultaneously by adjacent and parallel positioning of tubes, which were wrapped between the two elements of a 16-channel flexible measurement coil (Variety, NORAS MRI products). Measurements were performed with a clinical 3 T whole-body MRI scanner (MAGNETOM Prisma, Siemens Healthineers). Samples were placed with the fiber orientation parallel to the main magnetic field to reduce the influence of magic angle effects on T_2^* relaxation times⁴⁶. To mitigate the problem of rapid signal decay of tendon tissue, an in-house developed 3D UTE imaging sequence was used⁴⁷. To estimate longitudinal T_1 relaxation times, repeated 3D UTE acquisitions were performed using the variable flip angle (VFA) technique⁴⁸, with eight different excitation flip angles between 5° and 39° , an echo-time (TE) of 0.150 ms and a repetition time (TR) of 5.5 ms. The transverse relaxation time T_2^* was estimated by acquiring eight gradient-recalled echoes at different TEs between 0.150 ms and 3.0 ms by combining echo-train shifting⁴⁹ and multiple gradient refocused echoes within each readout train⁵⁰ and using a constant flip angle of 8° with TR of 6.0 ms. Other acquisition parameters were identical for both T_1 and T_2^* : isotropic spatial resolution $0.8 \times 0.8 \times 0.8$ mm³, 941 Hz/pixel acquisition bandwidth and two averages for improved signal-to-noise ratio. Images were reconstructed offline in Matlab (The MathWorks) using re-gridding with iterative sampling density compensation and an optimized kernel⁵¹. Data analysis and non-linear curve fitting to estimate relaxation parameters were also performed in Matlab. After calculating relaxation parameter maps, circular/elliptical regions of interest (ROI) were drawn manually in the central transverse slice of each disk. The T_1 and T_2^* relaxation times extracted from all voxels were averaged for each ROI.

Swelling measurements

Gravimetric swelling was measured using a calibrated balance with 0.001 g accuracy (LC621S, Sartorius). The fresh mass of a sample was measured immediately after sample dissection. For swelling curves,

swelling was recorded for 28 h with repeated measurements of five samples per condition (i.e., HYPO and ISO) from one animal. For the swollen state measurement, excess fluid was removed by gently patting the lower edge of the ECM samples onto a sheet of paper. Swelling was defined as $swelling (\%) = (m_{swollen} - m_{fresh})/m_{fresh}$.

Histological analysis of tissue organization

Representative samples from FRESH, HYPO and ISO conditions were embedded in fresh freezing compound (Tissue-Tek® O.C.T.™ Sakura) and frozen in liquid nitrogen-cooled isopentane (Carl Roth, Germany). Subsequently, frozen samples were stored at -80 °C until cryo sectioning. Samples were sectioned at 7 μm thickness and sections were placed onto glass slides (SuperFrost Ultra Plus, Menzel-Gläser). Histological analysis was performed by hematoxylin eosin (H&E) and Alcian blue (AB) staining. Imaging was performed using bright field microscopy at 20X magnification.

MRI high resolution structural imaging

High-resolution structural imaging was performed on representative ECM samples first in FRESH and then again after 24 h swelling in HYPO and ISO conditions using a 9.4 T MR small animal scanner (BioSpec USR 94/20, Bruker) with a horizontal bore of 20 cm, gradient system of 660 mT/m and ParaVision 6.0.1 operating software (BioSpin, Bruker). In addition, a vendor supplied two-channel quadrature cryoprobe was used to optimize the signal-to-noise ratio. Samples were deliberately oriented along the magic angle using a custom 3D printed laboratory tube insert with planes angled at 54.7°. Images were acquired using a vendor supplied 2D multi-slice Cartesian gradient-echo sequence with 70 x 70 μm² in-plane spatial resolution, 3.1 ms TE, 1200 ms TR, 8 averages, 75° excitation flip angle, 100 kHz acquisition bandwidth, 32 slices with a thickness of 200 μm and a total acquisition time of 35 minutes. Voxels with high signal intensity (light color) corresponded to regions in the tissue with increased water accumulation.

Biomechanical testing

ECM viscoelastic properties were quantified by elastic modulus and stress relaxation time by uniaxial unconfined compression (TestBench LM1 system, BOSE) using a 250 g load cell (Model 31 Low, Honeywell)². The compression step was conducted with minimal pre-load, at 0.016 mm/s and to a maximum strain of 15 % along the longitudinal axis of the cylindrical samples. A sample was characterized only once. The loading direction was aligned with the overall ECM fiber orientation to minimize effects of fiber tensile loading and focus on effects of PG-dominated water-binding on ECM viscoelasticity. At maximum compression, the stamp position was held constant to record the stress relaxation. The cross-sectional area of a sample was measured from images acquired with a 1200 dpi resolution with a digital scanner (1200 dpi, Perfection V200, Epson) using ImageJ software. The maximum compression was limited to 15% strain of tissue sample height²⁰, which is in the range of strains typically exerted by cells on their surrounding ECM⁵². The elastic modulus E was calculated from the slope of a 5% interval of the linear region of the stress strain curve. The stress relaxation behavior was quantified with $\tau_{0.50}$ and $\tau_{0.65}$ which were defined by the time until 50% and 35%, respectively, of the peak stress at maximum compression was released. The testing protocol restricted the recording of stress relaxation times to 500 s, as it was previously shown that $\tau_{0.50} \geq 500$ s of viscoelastic ECM affects cell-matrix interactions similar to (non-relaxing) elastic ECM²⁰. Considering that cells sense and respond to fast ECM stress relaxation properties when applying traction forces at ~s and ~min timescales⁵³, we introduced $\tau_{0.65}$ to analyze the early stress relaxation behavior. $\tau_{0.50}$ was reported to facilitate relating the results to those of other studies as it is a frequently used read-out in the biomaterials and tissue engineering community²⁰.

Osmotic gradient and ion diffusion measurements

ECM samples were dissected as described above from fresh Achilles tendons that were excised from five healthy sheep (male, 3 y) immediately after euthanasia at a local abattoir. Four tendons from two of the animals were used for osmotic gradient studies. Defined hypo-osmolar conditions were achieved by diluting saline solution used for ISO condition with deionized water in 25% increments. Osmolality was measured using a freezing-point osmometer (OSMOMAT Auto, Gonotec). ECM samples were exposed individually to the solutions in 2 ml tubes for 24 h and at the same sample to fluid volume ratio as described above. Subsequently, solution osmolality was measured again to determine osmolality changes due to ion efflux from samples. Viscoelasticity was quantified using uniaxial compression, as described above. ECM samples were freeze-dried to measure their dry weight and normalize changes in solution osmolality and obtain normalized ion efflux. For ion diffusion measurements, ECM samples were dissected from the other three animals as described above and subsequently, exposed to HYPO and ISO solutions. Solution osmolality was measured at baseline before (base) and after 24 h exposure (24h) of the ECM samples. To measure the efflux of selected monovalent and divalent ions from ECM samples, HYPO and ISO solutions were analyzed after 24 h. Ion concentrations were quantified using the ion selective electrode method for Na, Cl and K and photometric assay for Ca and Mg.

Collagen fiber contraction analysis

The SAXS measurements were performed with a Bruker Nanostar 2 using a 2D Vantec-2000 maintenance-free detector at a wavelength of 1.5418 Å (Cu K α). The focal spot size of the beam was 115 μ m and the sample-detector distance 28.10 cm. We measured the SAXS signal for three samples per condition at five randomly chosen points per condition. ECM samples were dissected from tendons of three animals. These were the contralateral tendons from the animals use for ion diffusion measurements, as described above, and assumed to have comparable tissue properties.

Statistical analysis and plotting

To analyze swelling over time, two-way analysis of variance (ANOVA) with Tukey's multiple comparison test was used. To analyze differences between a reference condition and a modulated condition, two-tailed paired t-test was used if values were normally distributed (e.g., for FRESH versus ISO, HYPO versus ISO, versus ISO+100); otherwise, Wilcoxon matched-pairs signed rank test was used. Correlations between variables were computed with the Pearson correlation coefficient r ; for experiments with less than eight ECM samples per condition, Spearman r was used. To analyze differences in *SwellChar*, two-tailed unpaired t-test was used. Statistical significance was set at $p < 0.05$ and different p values were indicated by *, **, *** and **** for $p < 0.05$, $p < 0.01$, $p < 0.001$ and $p < 0.0001$, respectively. In box plots, box limits show 25th and 75th percentiles, box middle lines show medians, and whiskers show minimum and maximum values. Bar plots show mean + / - standard deviation. Plots of simple linear regression show 95% confidence intervals as dotted black lines. Statistical analysis was performed with GraphPad Prism (version 8.3.0).

Data availability

The data supporting the presented findings are included in the main text of this paper as well as its supplementary information section. For research purposes and upon reasonable request, the corresponding author can provide all raw and analyzed datasets.

Code availability

The code used to analyze mechanical and MRI data in Matlab can be provided by the corresponding author upon reasonable request.

Competing interests declaration

None of the authors have competing financial or non-financial interests.

Acknowledgements

The authors thank Dag Wulsten for technical assistance with biomechanical characterization; Gabriela Korus for technical assistance with histology; Svenja Kassermann, Heilwig Fischer and Katja Reiter for technical assistance with tissue harvesting; Daniel Werner for technical assistance with XRD experiments; Tobias Gehlen for assistance with patient recruitment and scheduling; Rainald Ehrig for technical assistance with data analysis; and David Mooney, Franka Klatte-Schulz, Laia Albiol and Alison Agres for sharing their expertise and insights within the context of this work. This work was supported by the German Research Foundation (Deutsche Forschungsgemeinschaft; DU 298/25-1, RE 1123/22-1, KR 4783/2-1, BR 6698/1-1, SFB 1444).

References

1. Fullerton, G. D. & Amurao, M. R. Evidence that collagen and tendon have monolayer water coverage in the native state. *Cell Biol. Int.* **30**, 56–65 (2006).
2. Mow, V. C., Ratcliffe, A. & Robin Poole, A. Cartilage and diarthrodial joints as paradigms for hierarchical materials and structures. *Biomaterials* **13**, 67–97 (1992).
3. Ehrlich, S. *et al.* The osmotic pressure of chondroitin sulphate solutions: Experimental measurements and theoretical analysis. *Biorheology* **35**, 383–397 (1998).
4. Schwartz, N. B. & Domowicz, M. S. Proteoglycans in brain development and pathogenesis. *FEBS Lett.* **592**, 3791–3805 (2018).
5. Gordon, A. M., Huxley, A. F. & Julian, F. J. The variation in isometric tension with sarcomere. *J. Physiol.* **184**, 170–192 (1966).
6. Gill, S., Wight, T. N. & Frevert, C. W. Proteoglycans: Key regulators of pulmonary inflammation and the innate immune response to lung infection. *Anat. Rec.* **293**, 968–981 (2010).
7. Wiig, H. Pathophysiology of tissue fluid accumulation in inflammation. *J. Physiol.* **589**, 2945–2953 (2011).
8. Hashemi, H. S. *et al.* Assessment of Mechanical Properties of Tissue in Breast Cancer-Related Lymphedema Using Ultrasound Elastography. *IEEE Trans. Ultrason. Ferroelectr. Freq. Control* **66**, 541–550 (2019).
9. Nia, H. T. *et al.* Solid stress and elastic energy as measures of tumour mechanopathology. *Nat. Biomed. Eng.* (2017) doi:10.1038/s41551-016-0004.
10. Nikitovic, D. *et al.* Proteoglycans-Biomarkers and targets in cancer therapy. *Front. Endocrinol. (Lausanne)*. **9**, 1–8 (2018).
11. Nia, H. T., Munn, L. L. & Jain, R. K. Physical traits of cancer. *Science (80-.)*. **370**, (2020).
12. Hsu, C. K. *et al.* Mechanical forces in skin disorders. *J. Dermatol. Sci.* **90**, 232–240 (2018).
13. Varedi, M., Tredget, E. E., Ghahary, A. & Scott, P. G. Stress-relaxation and contraction of a collagen matrix induces expression of TGF- β and triggers apoptosis in dermal fibroblasts. *Biochem. Cell Biol.* **78**, 427–436 (2000).
14. Masic, A. *et al.* Osmotic pressure induced tensile forces in tendon collagen. *Nat. Commun.* **6**, 1–8 (2015).
15. Dolega, M. E. *et al.* Extra-cellular matrix in multicellular aggregates acts as a pressure sensor controlling cell proliferation and motility. *Elife* **10**, 1–33 (2021).
16. Li, Y. *et al.* Compression-induced dedifferentiation of adipocytes promotes tumor progression. *Sci. Adv.* **6**, (2020).
17. Lee, H. pyo, Stowers, R. & Chaudhuri, O. Volume expansion and TRPV4 activation regulate stem cell fate in three-dimensional microenvironments. *Nat. Commun.* **10**, (2019).
18. Murray, J. F. INT J TUBERC LUNG DIS 15(2):155-160 Pulmonary edema: pathophysiology and diagnosis. *Int. J. Tuberc. Lung Dis.* **15**, 155–160 (2011).
19. Vining, K. H. & Mooney, D. J. Mechanical forces direct stem cell behaviour in development and

- regeneration. *Nature Reviews Molecular Cell Biology* (2017) doi:10.1038/nrm.2017.108.
20. Chaudhuri, O. *et al.* Hydrogels with tunable stress relaxation regulate stem cell fate and activity. *Nat. Mater.* **15**, 326–334 (2016).
 21. Chaudhuri, O., Cooper-White, J., Janmey, P. A., Mooney, D. J. & Shenoy, V. B. Effects of extracellular matrix viscoelasticity on cellular behaviour. *Nature* **584**, 535–546 (2020).
 22. Fullerton, G. D. & Rahal, A. Collagen structure: The molecular source of the tendon magic angle effect. *J. Magn. Reson. Imaging* **25**, 345–361 (2007).
 23. Nebelung, S. *et al.* Ex vivo quantitative multiparametric MRI mapping of human meniscus degeneration. *Skeletal Radiol.* **45**, 1649–1660 (2016).
 24. Ma, Y. J., Chang, E. Y., Bydder, G. M. & Du, J. Can ultrashort-TE (UTE) MRI sequences on a 3-T clinical scanner detect signal directly from collagen protons: freeze–dry and D2O exchange studies of cortical bone and Achilles tendon specimens. *NMR Biomed.* (2016) doi:10.1002/nbm.3547.
 25. Bachmann, E. *et al.* T1-and T2*-Mapping for Assessment of Tendon Tissue Biophysical Properties: A Phantom MRI Study. *Invest. Radiol.* (2019) doi:10.1097/RLI.0000000000000532.
 26. Rorschach, H. E., Lin, C. & Hazlewood, C. F. Diffusion of water in biological tissues. *Scanning Microsc.* **5**, (1991).
 27. Andreisek, G. & Weiger, M. T2* mapping of articular cartilage: current status of research and first clinical applications. *Invest. Radiol.* **49**, 57–62 (2014).
 28. Thorpe, C. T. & Screen, H. R. C. Tendon Structure and Composition. *Adv. Exp. Med. Biol.* **920**, 3–10 (2016).
 29. Werbner, B. *et al.* Saline-polyethylene glycol blends preserve in vitro annulus fibrosus hydration and mechanics: An experimental and finite-element analysis. *J. Mech. Behav. Biomed. Mater.* **125**, 104951 (2021).
 30. Fernández-Sánchez, M. E. *et al.* Mechanical induction of the tumorigenic β -catenin pathway by tumour growth pressure. *Nature* (2015) doi:10.1038/nature14329.
 31. Masic, A. *et al.* Multiscale Analysis of Mineralized Collagen Combining X-ray Scattering and Fluorescence with Raman Spectroscopy under Controlled Mechanical, Thermal, and Humidity Environments. *ACS Biomater. Sci. Eng.* **3**, 2853–2859 (2017).
 32. Ping, H. *et al.* Mineralization generates megapascal contractile stresses in collagen fibrils. *Science* **376**, 188–192 (2022).
 33. Horkay, F., Bassar, P. J., Hecht, A. M. & Geissler, E. Chondroitin sulfate in solution: Effects of mono- and divalent salts. *Macromolecules* **45**, 2882–2890 (2012).
 34. Inoue, N. & Espinoza Orías, A. A. Biomechanics of Intervertebral Disk Degeneration. *Orthop. Clin. North Am.* **42**, 487–499 (2011).
 35. Streitberger, K. J. *et al.* High-resolution mechanical imaging of glioblastoma by multifrequency magnetic resonance elastography. *PLoS One* **9**, (2014).
 36. Safar, M. E. Arterial stiffness as a risk factor for clinical hypertension. *Nat. Rev. Cardiol.* **15**, 97–105 (2018).
 37. Engler, A. J., Sen, S., Sweeney, H. L. & Discher, D. E. Matrix Elasticity Directs Stem Cell Lineage

- Specification. *Cell* **126**, 677–689 (2006).
38. Brauer, E., Klein, O., Neblich, G., Duda, G. N. & Petersen, A. Fibrillar collagen amplifies and stores single cell tensile forces during tissue formation Keywords.
 39. Yalak, G. & Vogel, V. Extracellular phosphorylation and phosphorylated proteins: Not just curiosities but physiologically important. *Sci. Signal.* **5**, 1–14 (2012).
 40. Sussman, M. V. & Katchalsky, A. Mechanochemical turbine: A new power cycle. *Science (80-.)*. **167**, 45–47 (1970).
 41. Zhang, K., Feng, Q., Fang, Z., Gu, L. & Bian, L. Structurally Dynamic Hydrogels for Biomedical Applications: Pursuing a Fine Balance between Macroscopic Stability and Microscopic Dynamics. *Chem. Rev.* **121**, 11149–11193 (2021).
 42. Pownder, S. L., Shah, P. H., Potter, H. G. & Koff, M. F. The effect of freeze-thawing on magnetic resonance imaging T2* of freshly harvested bovine patellar tendon. *Quant. Imaging Med. Surg.* **5**, 368–36873 (2015).
 43. Fishbein, K. W. *et al.* Effects of formalin fixation and collagen cross-linking on T2 and magnetization transfer in bovine nasal cartilage. *Magn. Reson. Med.* **57**, 1000–1011 (2007).
 44. Money, N. P. Osmotic Pressure of Aqueous Polyethylene Glycols. *Plant Physiol.* (1989) doi:10.1104/pp.91.2.766.
 45. Herrmann, K. H., Gärtner, C., Güllmar, D., Krämer, M. & Reichenbach, J. R. 3D printing of MRI compatible components: Why every MRI research group should have a low-budget 3D printer. *Med. Eng. Phys.* (2014) doi:10.1016/j.medengphy.2014.06.008.
 46. Bydder, M., Rahal, A., Fullerton, G. D. & Bydder, G. M. The magic angle effect: A source of artifact, determinant of image contrast, and technique for imaging. *Journal of Magnetic Resonance Imaging* (2007) doi:10.1002/jmri.20850.
 47. Herrmann, K. H., Krämer, M. & Reichenbach, J. R. Time efficient 3D radial UTE sampling with fully automatic delay compensation on a clinical 3T MR scanner. *PLoS One* (2016) doi:10.1371/journal.pone.0150371.
 48. Fram, E. K. *et al.* Rapid calculation of T1 using variable flip angle gradient refocused imaging. *Magn. Reson. Imaging* (1987) doi:10.1016/0730-725X(87)90021-X.
 49. Feinberg, D. A. & Oshio, K. Gradient-echo shifting in fast MRI techniques (ERASE imaging) for correction of field inhomogeneity errors and chemical shift. *J. Magn. Reson.* (1992) doi:10.1016/0022-2364(92)90246-4.
 50. Krämer, M. *et al.* Immersion of Achilles tendon in phosphate-buffered saline influences T1 and T2* relaxation times: An ex vivo study. *NMR Biomed.* (2020) doi:10.1002/nbm.4288.
 51. Zwart, N. R., Johnson, K. O. & Pipe, J. G. Efficient sample density estimation by combining gridding and an optimized kernel. *Magn. Reson. Med.* **67**, 701–710 (2012).
 52. Legant, W. R. *et al.* Measurement of mechanical tractions exerted by cells in three-dimensional matrices. *Nat. Methods* **7**, 969–971 (2010).
 53. Vogel, V. & Sheetz, M. Local force and geometry sensing regulate cell functions. *Nat. Rev. Mol. Cell Biol.* **7**, 265–275 (2006).

Figures

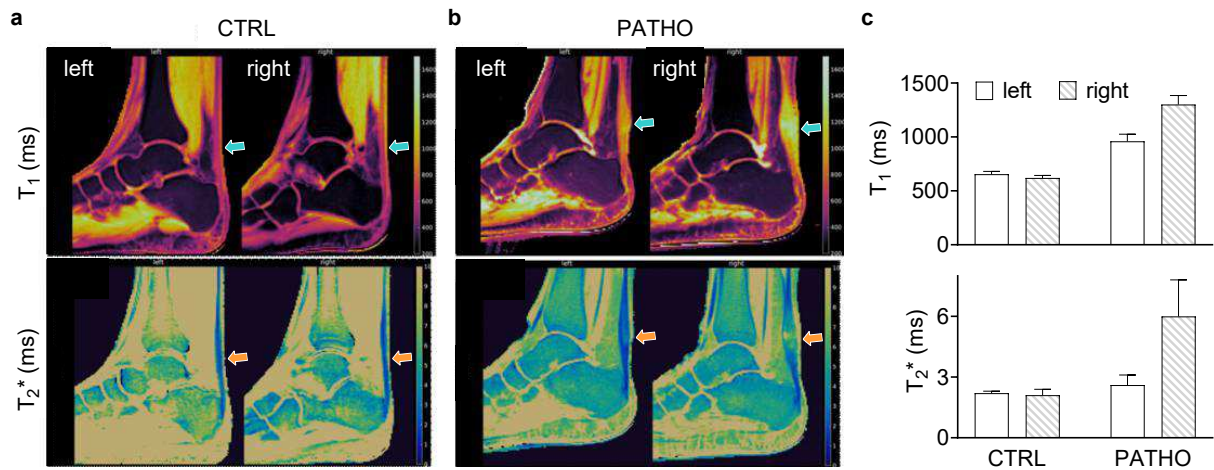


Fig. 1 | In vivo MRI scans of Achilles tendons showing swelling-related alterations in T_1 and T_2^* . Case study of clinical MRI scans of **a**, asymptomatic control subject (CTRL) versus **b**, patient (PATHO) with a diagnosed mechanopathology, mid-portion Achilles tendinopathy, in their right limb ($n=1$) with representative parameter maps of sagittal planes of T_1 (top row) and T_2^* (bottom row). **c**, Quantification of T_1 (top) and T_2^* (bottom) in the mid-portions of left and right Achilles tendons.

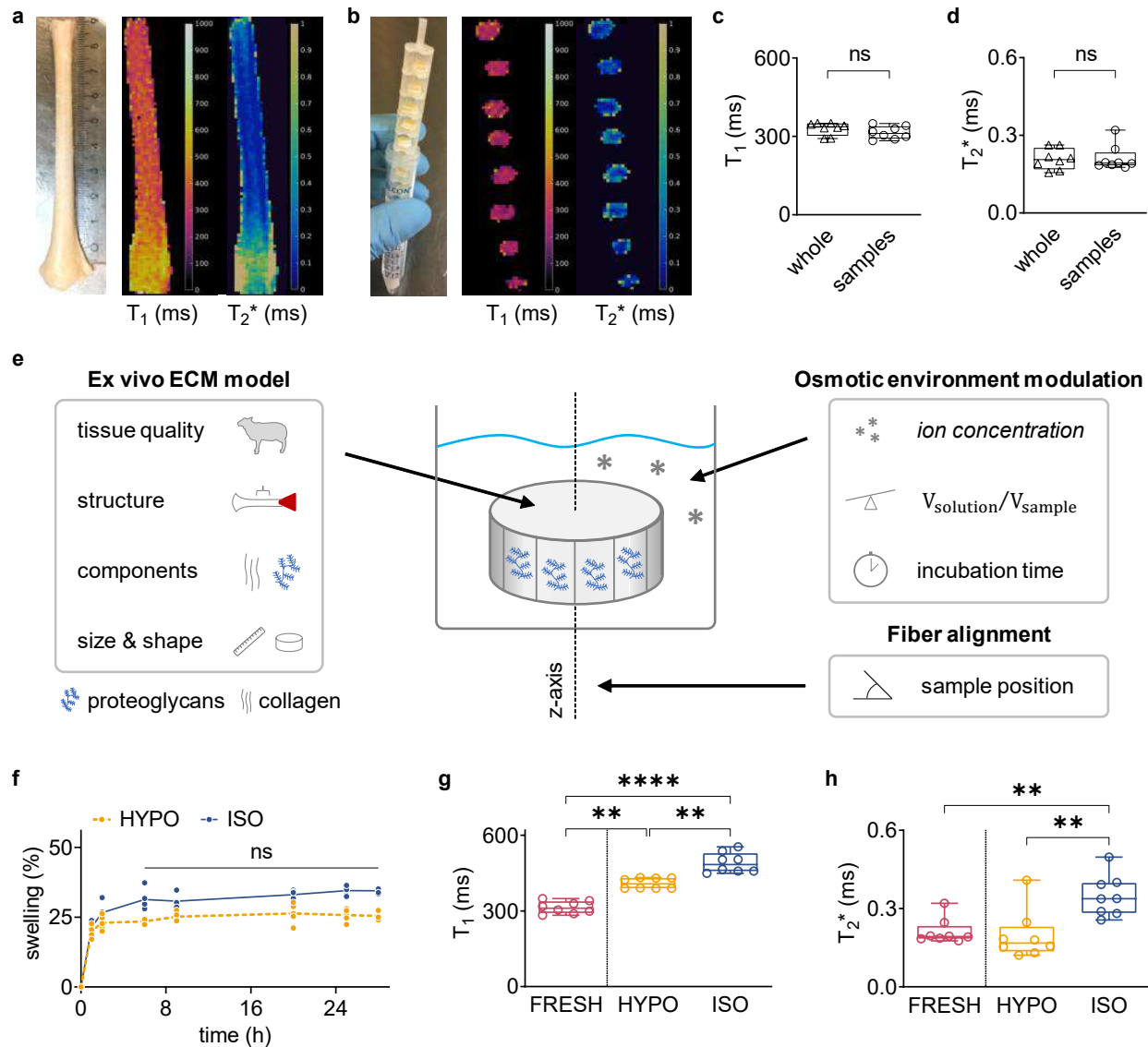


Fig. 2 | Physical ex vivo characterization of dissected Achilles tendon tissue showing that MRI T_1 and T_2^* detect osmotic environment-induced ECM alterations related to water binding. **a**, Representative image of Achilles tendon, T_1 and T_2^* maps of whole tendons. **b**, Left: Customized 3D printed sample mounting device enabled aligned ECM sample positioning and controlled exposure to different osmotic environments for multiple samples; right: representative T_1 and T_2^* maps of ECM samples in fresh (FRESH) condition. FRESH condition **c**, T_1 and **d**, T_2^* values in mid-portions of whole tendons versus dissected ECM samples revealed no significant differences. **e**, The developed ex vivo ECM model and experimental setup enabling to tune ECM properties by modulating the osmotic environment (e.g., by ion concentration). Other parameters of the ECM model (ex vivo ECM model), incubation condition (osmotic environment modulation) and sample positioning (fiber alignment) were kept consistent to enable reproducible MRI and mechanical characterization. **f**, Gravimetric swelling recorded over time of ECM samples exposed to HYPO and ISO solutions showed that approximate equilibrium was reached after 6 h of incubation. **g**, T_1 and **h**, T_2^* values of ECM samples in FRESH condition and after 24 h swelling in HYPO or ISO solution showed differences in water uptake characteristics depending on osmotic environment.

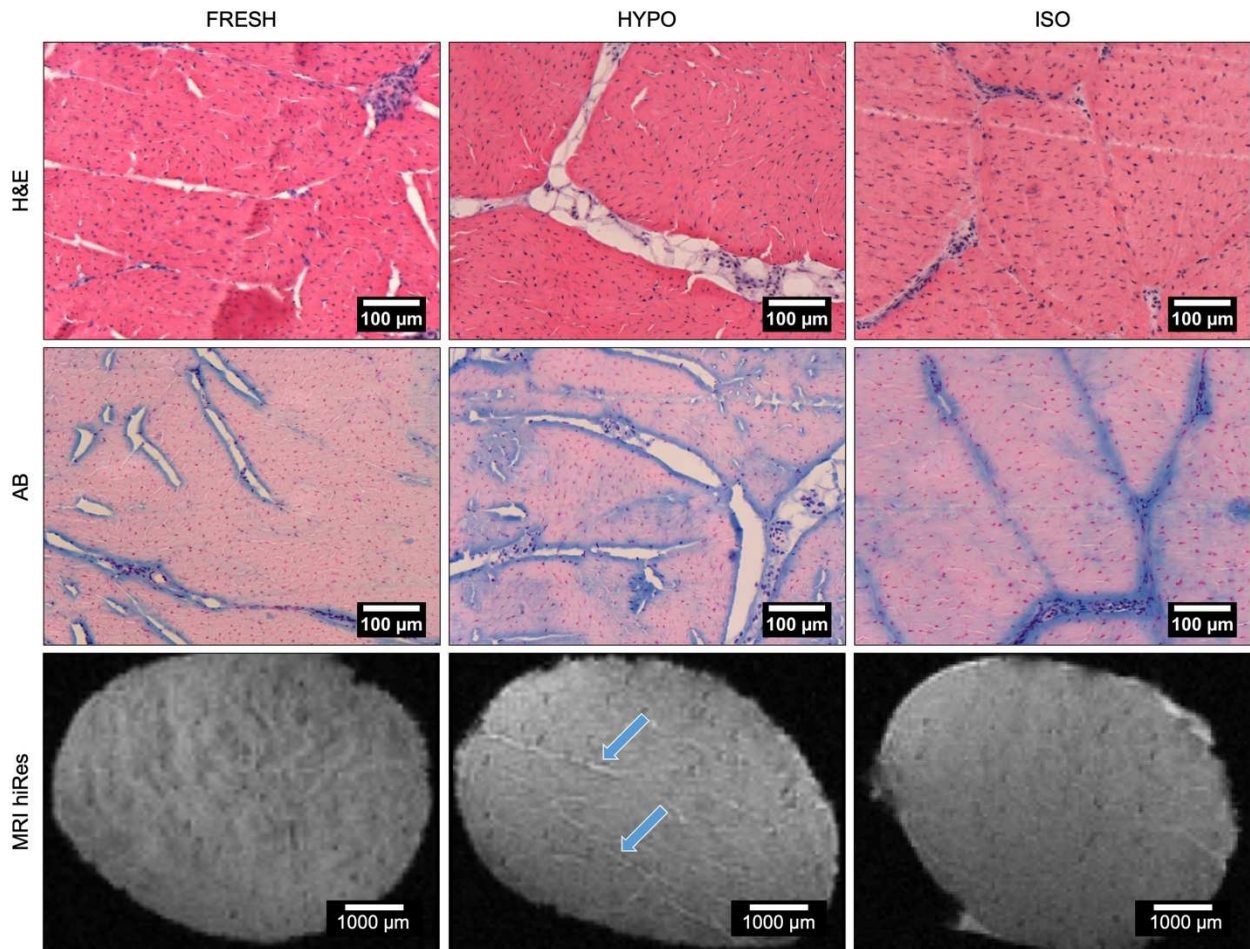


Fig. 3 | ECM stains of dissected mid-plane Achilles tendon cross sections showing structural alterations due to swelling and osmotic environment changes. Representative images of ECM cross sections of FRESH (left column), HYPO (middle column) and ISO (right column) conditions are shown. Histological stainings (top row) haematoxylin and eosin (H&E), showing collagen ECM in pink and cell nuclei as blue dots, and (middle row) Alcian blue (AB), showing proteoglycans in blue and cell nuclei in red, are presented. (MRI hiRes, bottom row) High resolution MR images were acquired using a 9.4 T scanner, showing white lines with increased signal intensities (blue arrows), indicating an increased amounts of accumulated water in the ECM. In AB images, increased blue staining in and along the intrafascicular (IF) matrix confirms high PG density in the IF matrix. Expanded IF regions in HYPO compared to FRESH and ISO conditions were visible in H&E and AB stainings and suggest increased PG water binding, which is supported by the white lines in MRI hiRes images that are similar in width to the IF regions in the H&E and AB stainings.

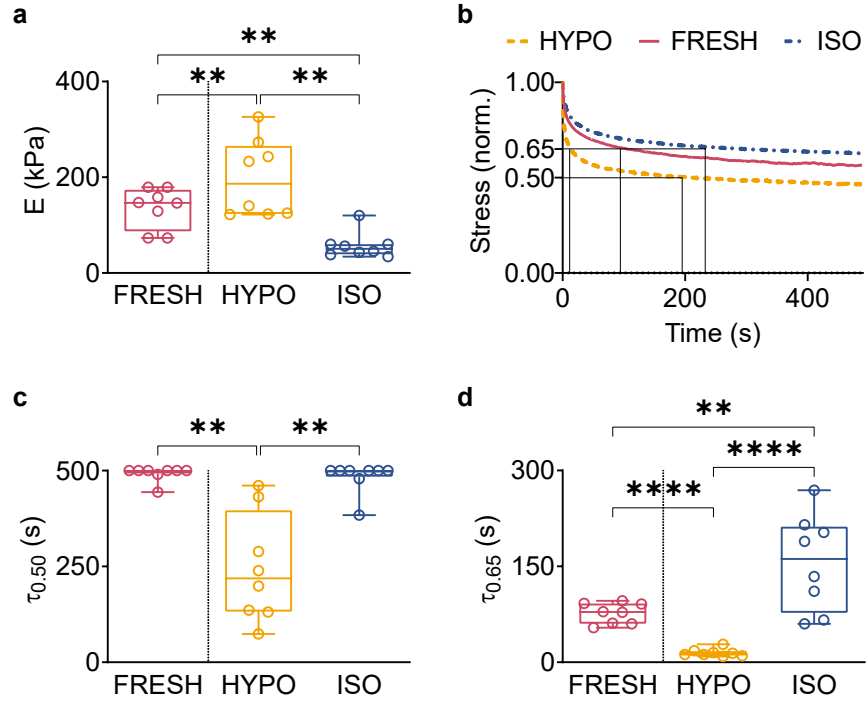


Fig. 4 | The ion concentration of the osmotic environment regulates the Achilles tendon ECM viscoelasticity ex vivo. Mechanical characterization of ECM samples was performed for FRESH, HYPO and ISO conditions. **a**, Elastic modulus E . The stress relaxation behavior is described by the relaxation of the applied peak stress at a maximum strain over time, which is shown with **b**, representative stress relaxation curves and quantified by **c**, $\tau_{0.50}$ and **d**, $\tau_{0.65}$, showing the time until 50% and 35%, respectively, of the peak stress was released.

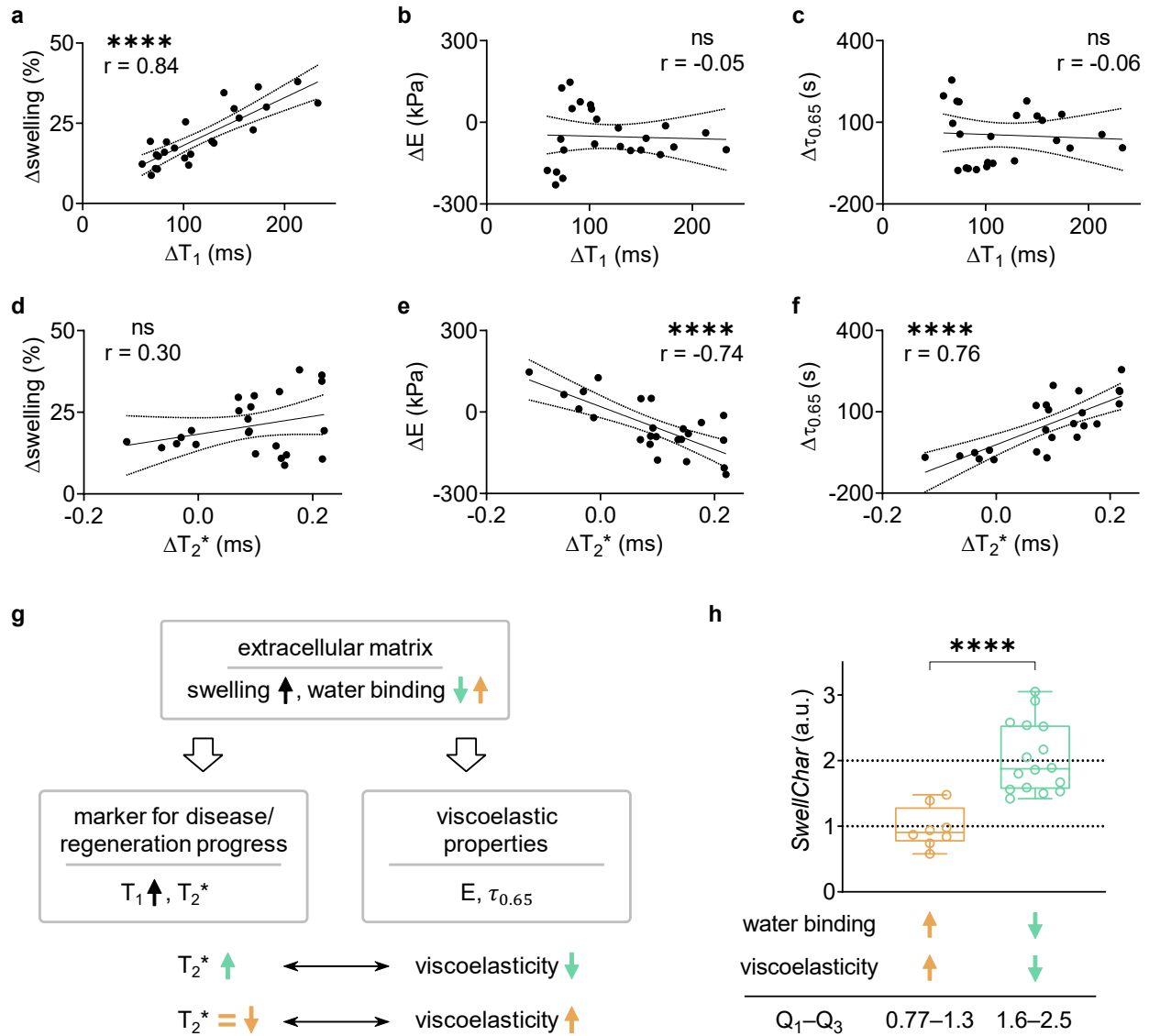


Fig. 5 | Combined MRI T_1 and T_2^* mapping reveal independent correlations that allow to distinguish between high and low water binding in swelling ECM and associated viscoelastic properties. Correlations based on observed changes, denoted by Δ , of each parameter between different conditions were quantified by Pearson r and shown for ΔT_1 with **a**, Δ swelling, **b**, ΔE and **c**, $\Delta\tau_{0.65}$, and for ΔT_2^* with **d**, Δ swelling, **e**, ΔE and **f**, $\Delta\tau_{0.65}$. **g**, Schematic illustrating the identified relationships between ECM swelling and water-binding strength to the clinically applicable MR relaxation parameters T_1 and T_2^* , and how their characteristic alterations offer insight into ECM viscoelastic properties E and $\tau_{0.65}$. **h**, The definition of the read-out $SwellChar$ allowed to distinguish between cases of high and low proportions of strongly bound water and associated changes in viscoelasticity for the present dataset using only one read-out parameter. Value ranges [Q_1-Q_3] for $SwellChar$ were found to be related to the distinct characteristics of water-binding strength and viscoelastic properties.

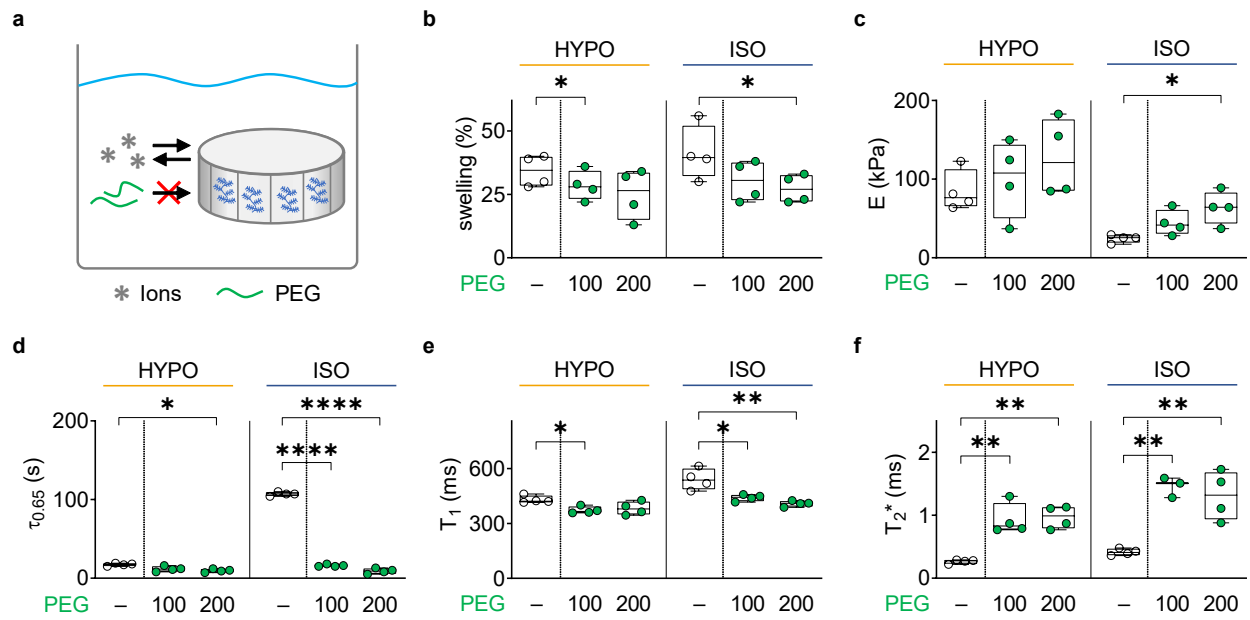


Fig. 6 | Application of osmotic pressure shows that dehydration-caused ECM alterations are different from effects of ion concentration tuned osmolality. **a**, Illustration of the differences between two types of osmolytes: ions can diffuse into ECM samples (Ions), while high molecular weight polyethylene glycol (PEG) cannot. Thus, added PEG applies osmotic pressure to an ECM sample which leads to its dehydration (i.e., decreased swelling). ECM samples were characterized by **b**, swelling, **c**, elastic modulus E , **d**, stress relaxation time $\tau_{0.65}$, **e**, T_1 and **f**, T_2^* values. Osmotic pressures of 100 and 200 kPa were applied by PEG (5,000 molecular weight) concentrations of 8 and 11 wt%, respectively.

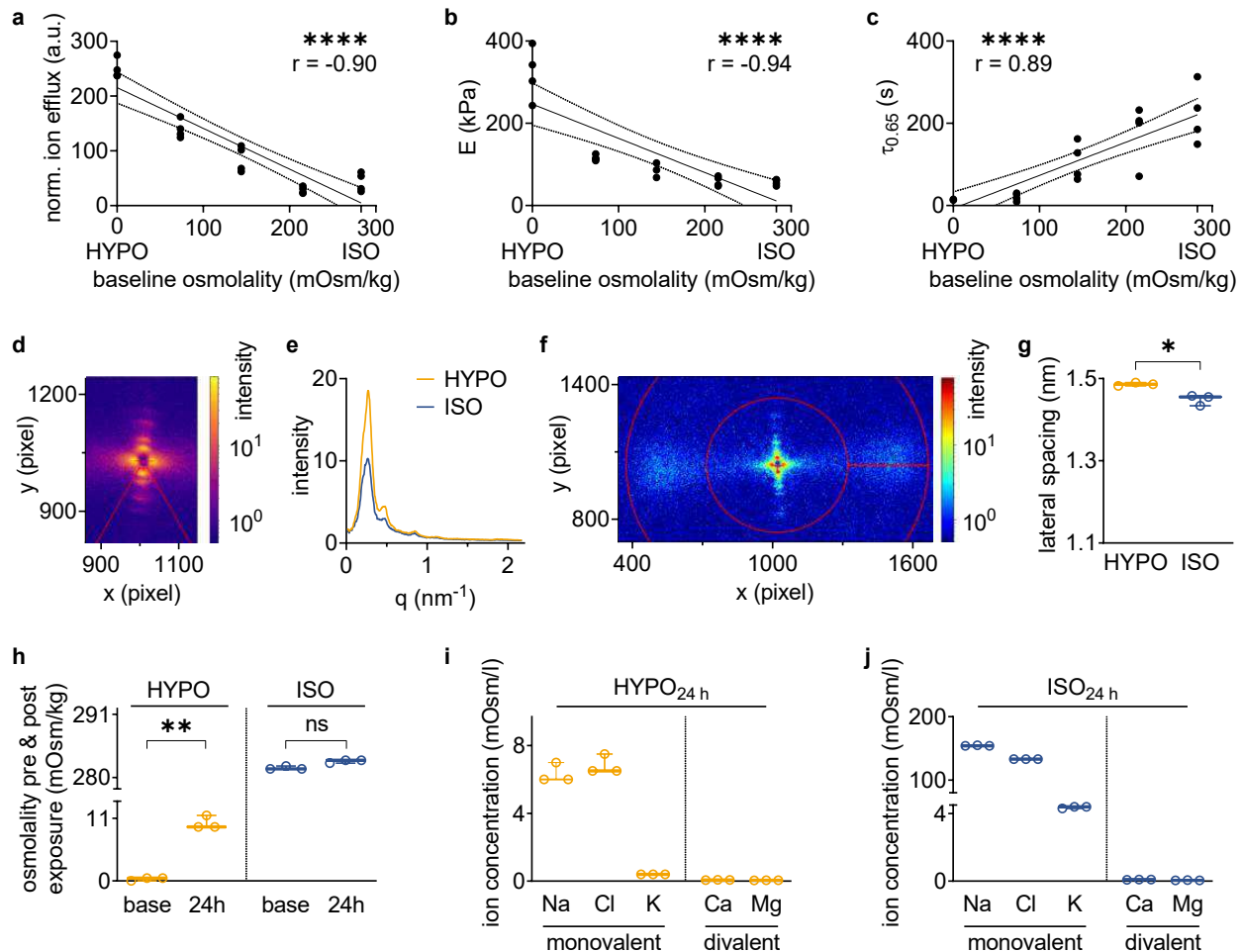


Fig. 7 | ECM viscoelasticity is regulated by the efflux of monovalent ions from ECM samples through affecting PG ion binding. A stepwise ion concentration gradient between HYPO and ISO was used to investigate changes to ECM samples after 24 h incubation. With increasingly hypo-osmolar conditions, we measured **a**, increased osmolality of the incubation solutions normalized by ECM sample dry weight (showing leakage of ions from ECM samples), **b**, increased elastic modulus E , and **c**, faster stress relaxation $\tau_{0.65}$ of ECM samples. Collagen axial staggering was analyzed from **d**, 2D SAXS patterns of Bragg peaks and revealed **e**, no shifts in intensity peaks. Analysis of collagen molecule lateral packing from **f**, 2D SAXS patterns revealed a slight increase of **g**, lateral molecule spacing within the range of hydrated collagen fibrils in HYPO condition, suggesting a slightly higher water uptake between collagen molecules. To further understand the role of PGs in the perifibrillar matrix, the diffusion of selected mono and divalent ions from the ECM samples in HYPO versus ISO environments was investigated. **h**, Solution osmolality pre- and post-incubation of ECM samples showed ion efflux in HYPO condition. **i**, After 24 h in HYPO, efflux of the monovalent Na and Cl ion was evident, while no change was observed for divalent Ca and Mg ions. **j**, After 24 h in ISO, Na and Cl were present in high concentrations, as expected, while Ca and Mg ions showed no efflux either, suggesting that these divalent ions remained bound inside the ECM samples.

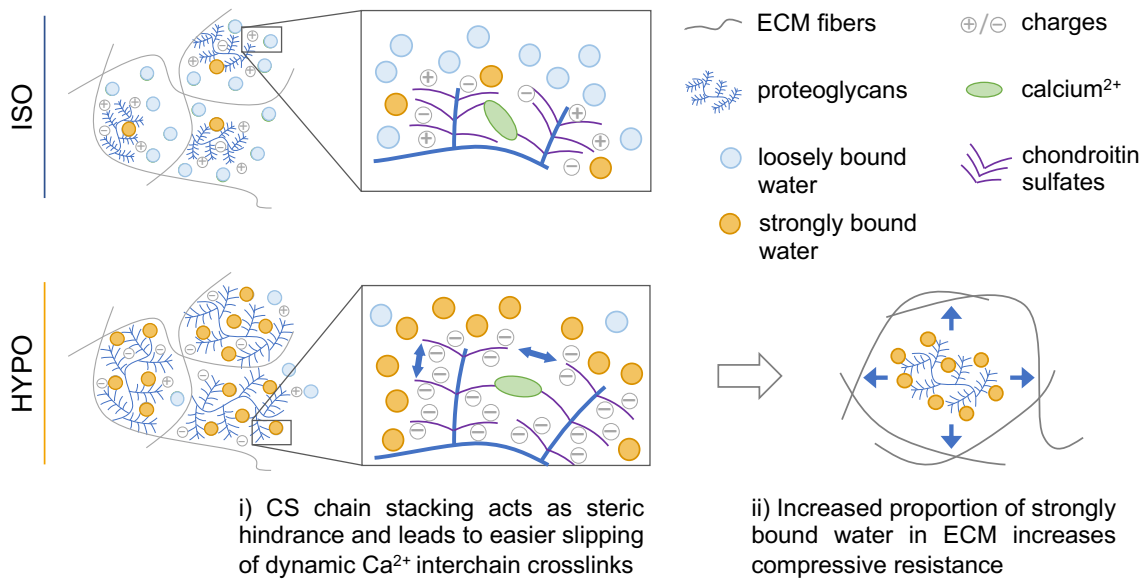
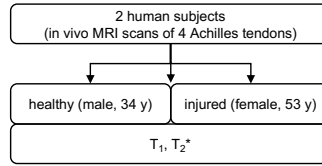


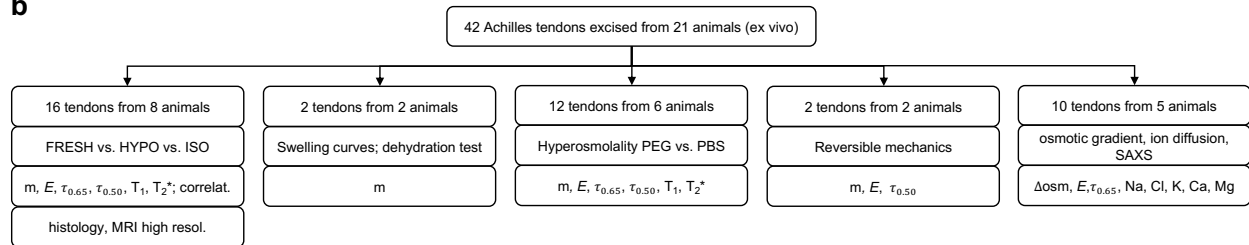
Fig. 8 | Proposed mechanism how PGs regulate ECM viscoelastic material properties, revealed by modulating the osmotic environment ion concentration. Compared to ISO, the proportion of loosely to strongly bound water in the ECM was higher in HYPO conditions. Ion diffusion experiments suggest increased negative charge of PGs due to leakage of cations from the ECM that would otherwise bind to the negatively charged PGs. Electrostatic repelling forces (two-headed blue arrows) acting between the more negatively charged PG subunits (e.g., chondroitin sulfate (CS) chains) can lead to CS chain stacking and thus increased distancing and enlarged PGs. i) The increased distancing can cause faster slipping of ionic (e.g., Ca²⁺) bonds between PGs under load. ii) ECM with more negatively charged PGs, binding more water strongly, increase the compressive resistance (one-headed blue arrows) of the ECM network under load.

Supplementary information

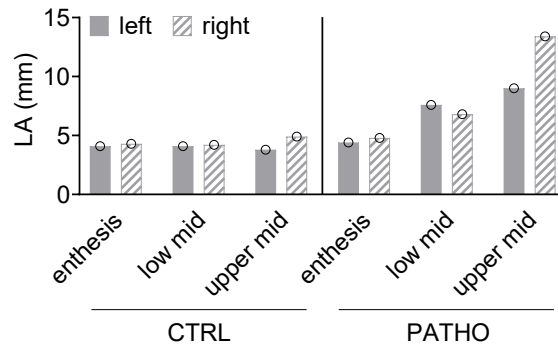
a



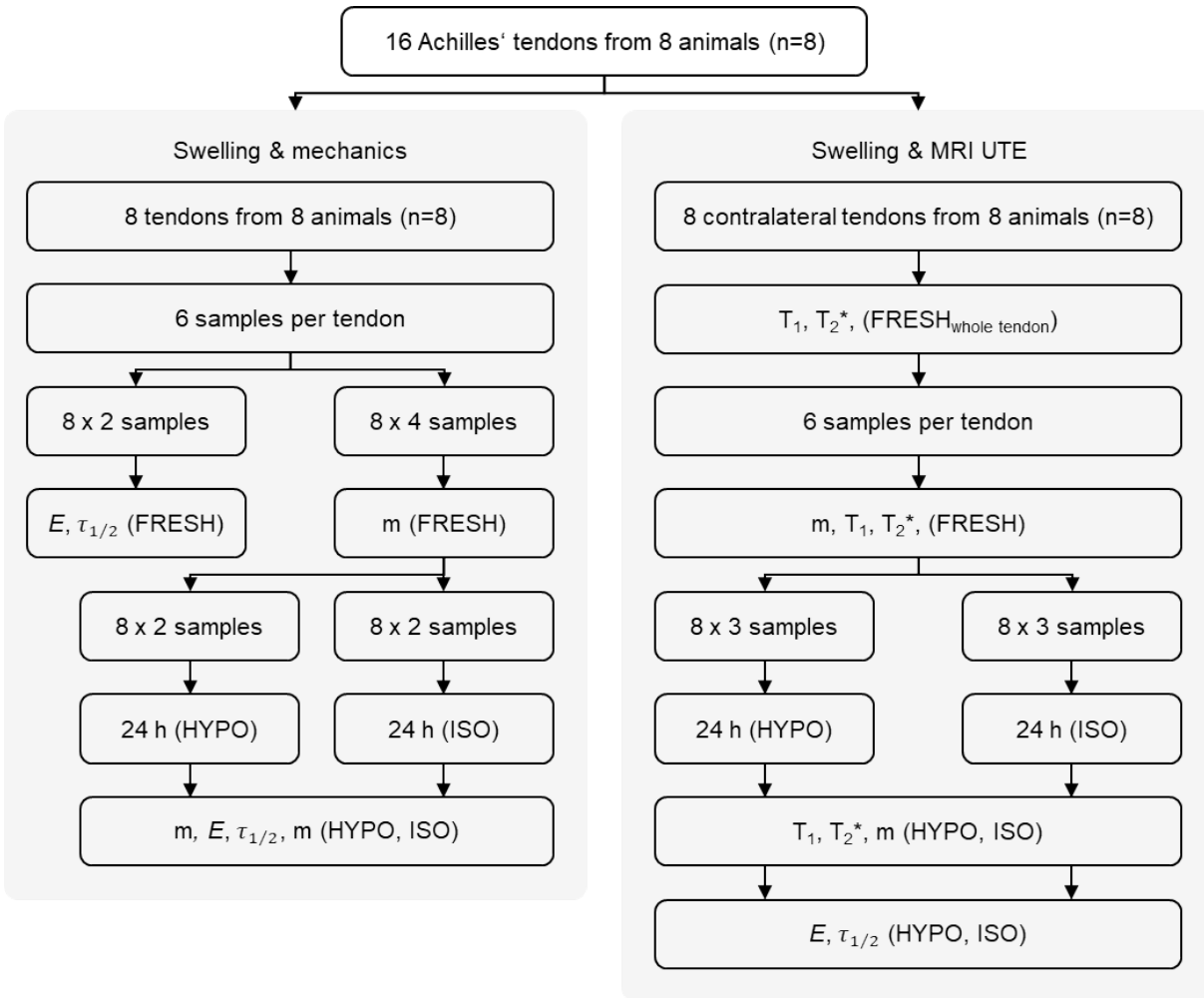
b



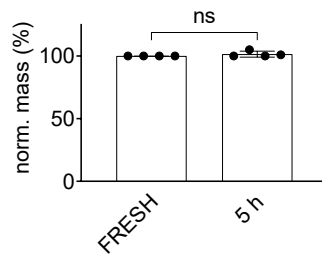
Supplementary Fig. 1 | Test subjects and ex vivo tissue used within the study. **a**, In vivo MRI scans were performed on two human subjects, including one asymptomatic control subject (CTRL, male, 34 y) and one patient (PATHO, female, 53 y) diagnosed with mid-portion Achilles tendinopathy. **b**, A total of 42 Achilles tendons from 21 sheep were used for the ex vivo model studies. Ex vivo tendons of 16 animals were excised from 4+ year old healthy female sheep, for osmotic gradient, ion diffusion and SAXS experiments, tendons of five animals were excised from 3+ year old healthy male sheep. Mid-portion Achilles tendon tissue properties of the male sheep were considered comparable with those of the female sheep. For each experiment, the number of tendons and animals used are listed together with the topic or conditions of the experiment and the quantified parameters. The quantified parameters were gravimetric swelling m , elastic modulus E , characteristic stress relaxation times $\tau_{0.65}$ and $\tau_{0.50}$, MR relaxation parameters T_1 and T_2^* , and independent correlations (correlat.). Structural analysis was performed using histology and high-resolution MRI.



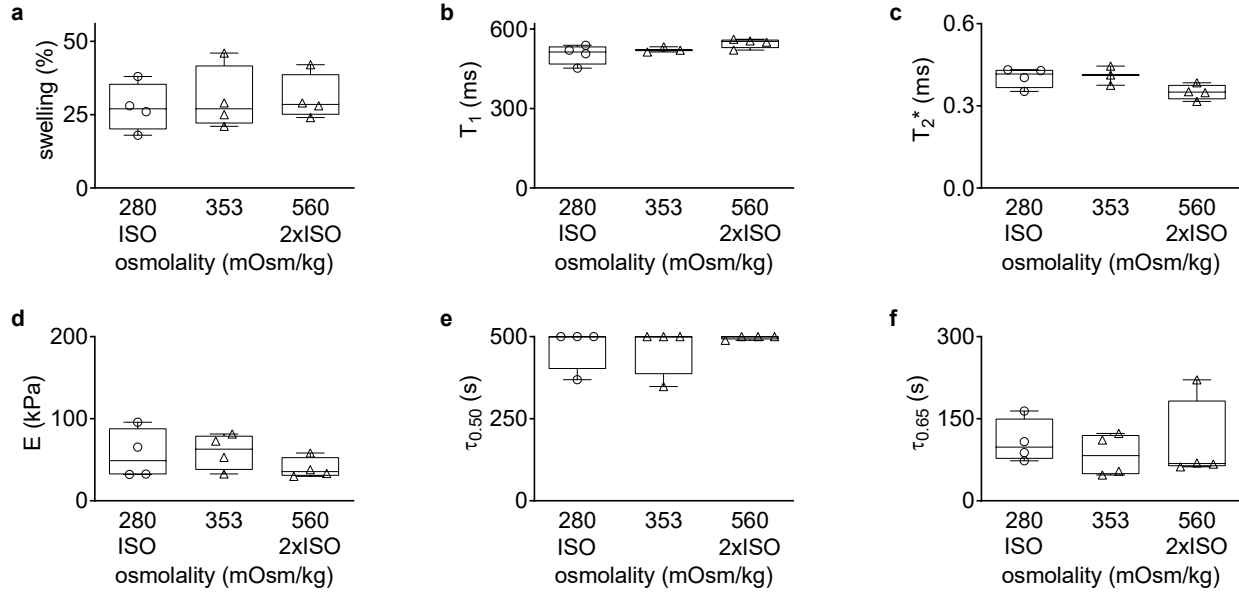
Supplementary Fig. 2 | Tendon size along the Achilles tendons computed from in vivo scans of an asymptomatic control subject (CTRL) compared with a patient (PATHO) with diagnosed mid-portion Achilles tendinopathy. Tendon size (i.e., thickness), quantified by the longest axis in a cross section (LA), was increased for the patient's tendon mid-portion and particularly on their right foot, where the tendinopathy was diagnosed. Increased tendon thickness on the patient's left foot may have been a result of abnormal loading due to pain avoidance gait.



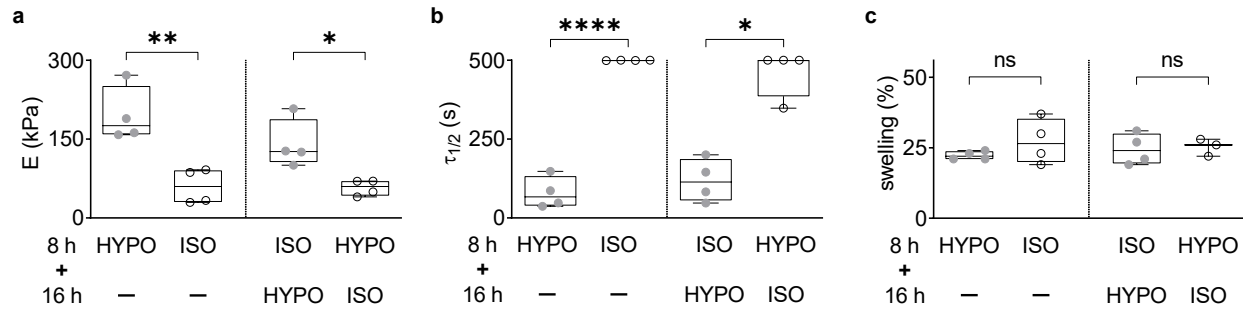
Supplementary Fig. 3 | Overview of the quantification study on the effects of different osmotic environments on ECM properties. The flowchart describes how samples were dissected from 16 Achilles tendons from 8 animals and subsequently divided into the 3 conditions of fresh state (FRESH), hypo-osmolar swelling (HYPO) and iso-osmolar swelling (ISO). Left: tendons used for mechanical characterization for viscoelasticity (E , $\tau_{1/2}$) and swelling (m). Right: contralateral tendons of each animal, assumed to have comparable tissue properties as ipsilateral tendons, and used for MRI UTE characterization for T_1 and T_2^* (whole tendons and dissected samples) and subsequent mechanical characterization for verification. If the alignment of a sample had significantly changed in the MRI scan (e.g., was strongly tilted), which was visible in the resulting parameter maps, its measured MRI values were excluded from analysis as the clearly altered fiber direction could affect the measured relaxation parameters (i.e., magic angle effects can affect T_2^* relaxation times ⁴⁶).



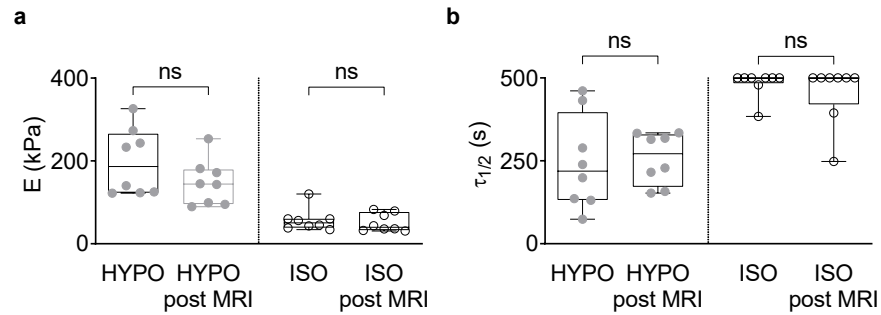
Supplementary Fig. 4 | Testing whether a moist environment in sealed tubes can prevent ECM sample dehydration for several hours to enable MRI scans of tendon in the fresh state. Mass of samples held in constant position by a 3D printed mounting device for 5 h in a sealed 15 ml tube with soaked gauze at the bottom of the tube normalized to the fresh condition weight (FRESH). Per condition, four samples from one animal were tested. Each samples was measured repeatedly: in the FRESH condition and after 5h in a sealed tube.



Supplementary Fig. 6 | Hyper-osmolar environments with osmolality increased by higher ion concentration showed a large proportion of loosely bound water in ECM in ISO condition (280 mOsm/kg). Both swelling and water binding as well as mechanics were not significantly affected, even by double ISO osmolality. This supports the design of the ex vivo ECM model and experimental setup, which used HYPO and ISO conditions as extreme comparisons of low and high proportions of loosely bound water, respectively. ECM samples were characterized by **a**, swelling, **b**, T_1 and **c**, T_2^* , **d**, elastic modulus E , **e**, stress relaxation time $\tau_{0.50}$ and **f**, $\tau_{0.65}$.



Supplementary Fig. 7 | Exposure of ECM samples to alternating osmolality indicates reversibility of mechanical changes. a, Elastic modulus E , **b**, stress relaxation half time $\tau_{1/2}$ and **c**, swelling; left: samples after incubation for 8 h in hypo-osmolar (HYPO) or iso-osmolar (ISO), right: samples initially subjected to swelling in one osmolality (HYPO or ISO) and then exposed to the other osmotic condition for another 16 h.



Supplementary Fig. 8 | Mechanical characterization after MRI analysis to verify the reproducibility and stability of ex vivo ECM tuning by changes of the osmotic environment ion concentration. Additional mechanical characterization of the contralateral tendons after MRI scans (MRI) shows the reproducibility of the experiments, as no significant differences were observed in comparison to the mechanical characterization of the ipsilateral tendons. This was tested for both for hypo-osmolar (HYPO) and iso-osmolar (ISO) swelling conditions, and proves the stability of the effect even at day 5 after tissue excision. The 5 days comprised 3 days of storage at 4°C and 2 days of incubation with one MRI scan in between. **a**, Elastic modulus E and **b**, stress relaxation half time $\tau_{1/2}$.